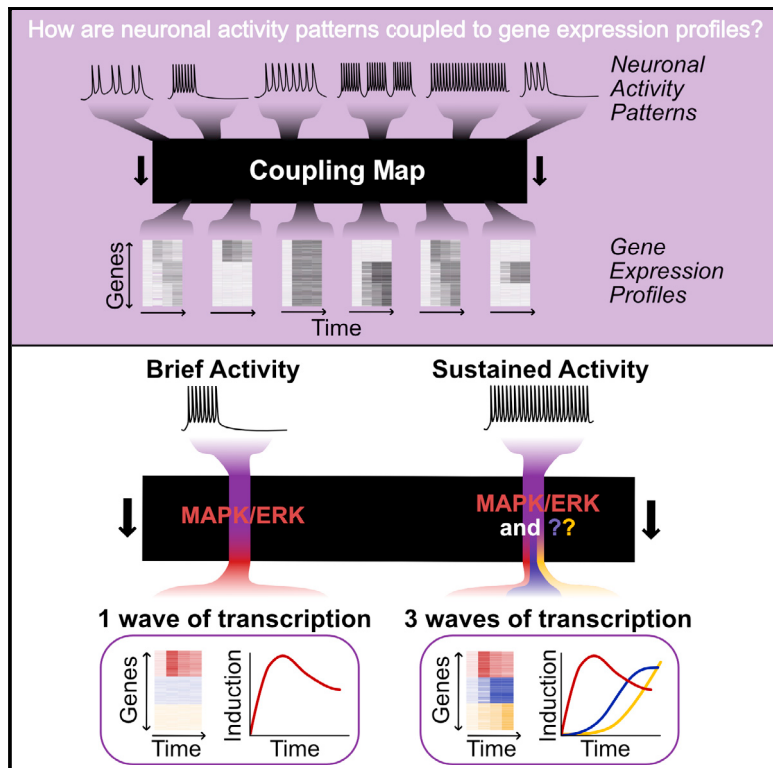


# Different Neuronal Activity Patterns Induce Different Gene Expression Programs

## Graphical Abstract



## Authors

Kelsey M. Tyssowski,  
Nicholas R. DeStefino,  
Jin-Hyung Cho, ..., Ramendra N. Saha,  
Serena M. Dudek, Jesse M. Gray

## Correspondence

rsaha3@ucmerced.edu (R.N.S.),  
dudek@niehs.nih.gov (S.M.D.),  
gray@genetics.med.harvard.edu (J.M.G.)

## In Brief

Tyssowski et al. report that different durations of neuronal activity induce different gene expression profiles, enabling inference of past neuronal activity from gene expression data. Furthermore, they show that MAPK/ERK signaling partially establishes this activity-pattern-to-gene-induction coupling.

## Highlights

- Distinct durations of neuronal activity induce different gene expression profiles
- Neuronal activity history can be inferred from gene expression
- Brief activity induces a gene set defined by sensitivity to MAPK/ERK signaling
- H3K27ac and eRNA induction are two separable steps of enhancer activation



# Different Neuronal Activity Patterns Induce Different Gene Expression Programs

Kelsey M. Tyssowski,<sup>1,6</sup> Nicholas R. DeStefino,<sup>1,6</sup> Jin-Hyung Cho,<sup>1</sup> Carissa J. Dunn,<sup>2</sup> Robert G. Poston,<sup>2</sup> Crista E. Carty,<sup>3</sup> Richard D. Jones,<sup>1</sup> Sarah M. Chang,<sup>1</sup> Palmyra Romeo,<sup>4</sup> Mary K. Wurzelmann,<sup>4</sup> James M. Ward,<sup>5</sup> Mark L. Andermann,<sup>3</sup> Ramendra N. Saha,<sup>2,4,7,\*</sup> Serena M. Dudek,<sup>4,7,\*</sup> and Jesse M. Gray<sup>1,7,8,\*</sup>

<sup>1</sup>Department of Genetics, Harvard Medical School, Boston, MA 02115, USA

<sup>2</sup>Molecular Cell Biology Unit, University of California Merced, Merced, CA 95343, USA

<sup>3</sup>Division of Endocrinology, Diabetes and Metabolism, Beth Israel Deaconess Medical Center, Harvard Medical School, Boston, MA 02115, USA

<sup>4</sup>Neurobiology Laboratory, National Institute of Environmental Health Sciences, National Institutes of Health, Research Triangle Park, NC 27709, USA

<sup>5</sup>Integrative Bioinformatics, National Institute of Environmental Health Sciences, National Institutes of Health, Research Triangle Park, NC 27709, USA

<sup>6</sup>These authors contributed equally

<sup>7</sup>Senior author

<sup>8</sup>Lead Contact

\*Correspondence: rsaha3@ucmerced.edu (R.N.S.), dudek@niehs.nih.gov (S.M.D.), gray@genetics.med.harvard.edu (J.M.G.)

<https://doi.org/10.1016/j.neuron.2018.04.001>

## SUMMARY

A vast number of different neuronal activity patterns could each induce a different set of activity-regulated genes. Mapping this coupling between activity pattern and gene induction would allow inference of a neuron's activity-pattern history from its gene expression and improve our understanding of activity-pattern-dependent synaptic plasticity. In genome-scale experiments comparing brief and sustained activity patterns, we reveal that activity-duration history can be inferred from gene expression profiles. Brief activity selectively induces a small subset of the activity-regulated gene program that corresponds to the first of three temporal waves of genes induced by sustained activity. Induction of these first-wave genes is mechanistically distinct from that of the later waves because it requires MAPK/ERK signaling but does not require *de novo* translation. Thus, the same mechanisms that establish the multi-wave temporal structure of gene induction also enable different gene sets to be induced by different activity durations.

## INTRODUCTION

Neurons induce hundreds of activity-regulated genes (ARGs) in response to elevations in their activity (Flavell and Greenberg, 2008), suggesting that a vast number of different neuronal firing patterns could each be coupled to a different gene expression profile. Consistent with this idea, distinct neuronal activity patterns differentially induce the expression of several individual genes (Douglas et al., 1988; Greenberg et al., 1986; Sheng et al., 1993;

Worley et al., 1993). However, single-gene studies are inadequate for creating a complete coupling map that relates each neuronal activity pattern to a corresponding gene expression profile. This coupling map would be powerful because it would allow inference of a neuron's activity history from its gene expression profile. This kind of inference could enable single-cell RNA-seq-based assessment of the activity histories of tens of thousands of neurons at a time, far more than can be assessed with electrical recording or calcium imaging (Hrvatin et al., 2018; Hu et al., 2017; Jun et al., 2017; Mohammed et al., 2016; Wu et al., 2017). To generate a coupling map, it will be necessary to make genome-scale comparisons of the ARGs induced by different activity patterns (Lee et al., 2017).

Transcriptional regulators could establish the coupling map, as they can both define specific ARG subsets and respond differentially to different activity patterns. Regulators that define ARG subsets include transcription factors, such as CREB and SRF, that bind the promoters and enhancers of only some ARGs (Kim et al., 2010). Regulators that respond differentially to different activity patterns include calcium-dependent cell-signaling pathways, such as the MAPK/ERK pathway (De Koninck and Schulman, 1998; Dolmetsch et al., 1998, 1997; Dudek and Fields, 2001; Eshete and Fields, 2001; Fields et al., 1997; Fujii et al., 2013; Ma et al., 2011; Wu et al., 2001a). Thus, each of the many inducible signaling pathways could regulate a distinct subset of ARGs, creating gene modules that are each independently coupled to activity patterns. Identifying the regulators of these gene modules would enable manipulation of the coupling map to investigate its contribution to firing-pattern-specific, gene-induction-dependent synaptic plasticity, such as long-term potentiation, long-term depression, and synaptic scaling (Ahn et al., 1999; Ibata et al., 2008; Nguyen et al., 1994).

One example of a regulatory mechanism that could couple stimulation patterns to induction of different gene modules comes from non-neuronal cells, where it has been proposed that brief and sustained stimulation differentially induce two of



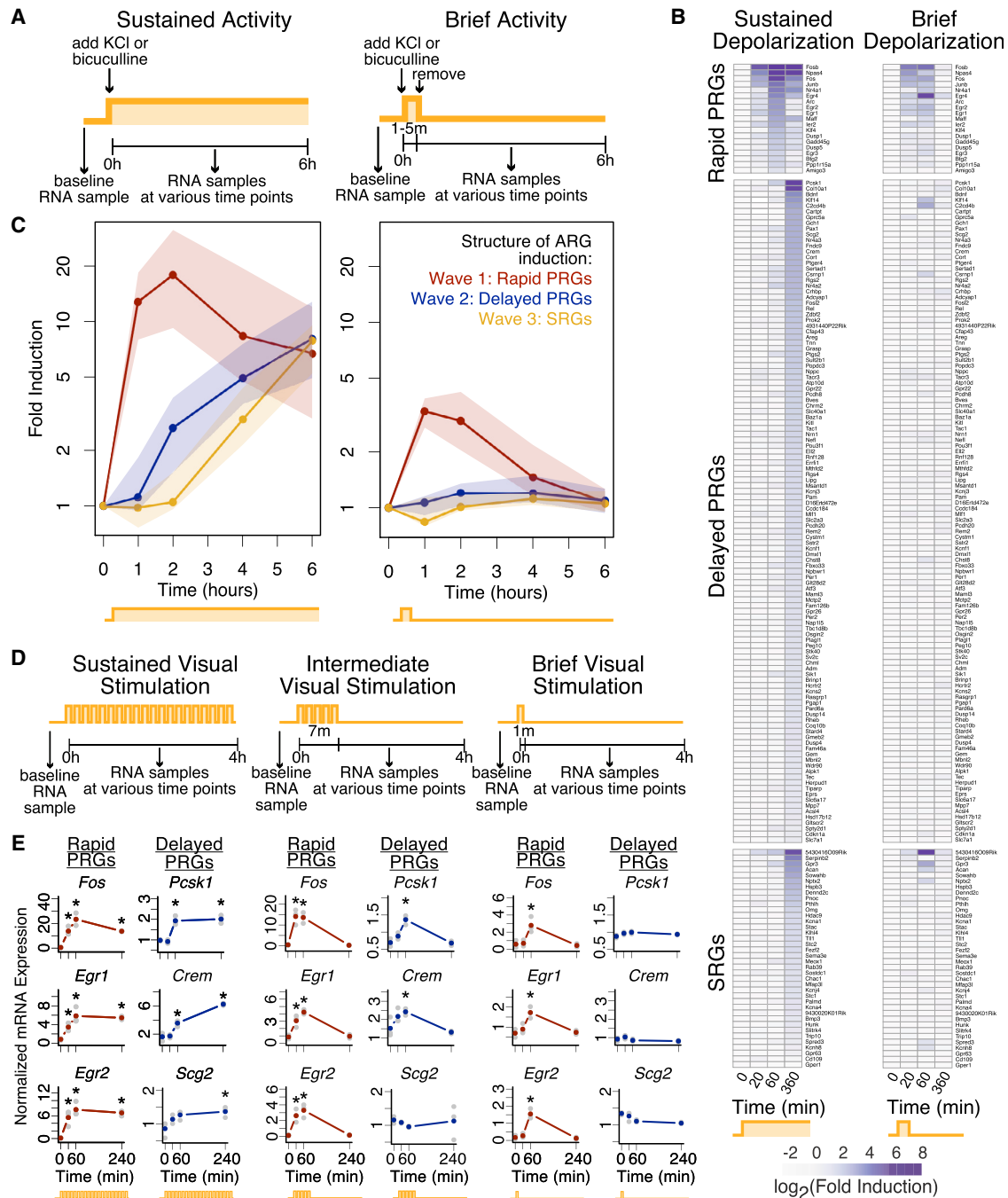


**Figure 1. Brief Neuronal Activation Selectively Induces the First of Three Waves of Gene Induction**

(A) Experimental system for comparing sustained and brief neuronal activation *in vitro*. Except where indicated otherwise, neuronal activation is accomplished with brief (1-min) or sustained KCl depolarization of cortical neurons silenced 14–16 hr before stimulation with APV and NBQX.

(B) Comparison of gene induction upon sustained or brief neuronal activation using activity-regulated gene-capture-based RNA sequencing (ARG-seq) (means,  $n = 3-6$  biological replicates). Only induced genes are shown. Gene categories are defined based on kinetics of gene induction as well as induction in the presence of the translation inhibitor cycloheximide (Figure S1B). Genes induced by brief neuronal activation are enriched for rPRGs ( $p < 10^{-13}$ , Fisher's exact test). PRG, primary response gene; SRG, secondary response gene; rPRGs, rapid PRGs.

(C) Three kinetically distinct temporal waves of gene induction as detected by high-throughput microfluidic qPCR. Points represent the mean expression of the median gene for each class. Shading covers the middle quartiles of mean expressions (25%–75%) ( $n = 6$  biological replicates). Each wave is kinetically distinct from the other waves (rPRG versus dPRG/SRG induction at 1 hr, dPRG versus SRG induction at 2 hr,  $p < 0.003$ , rank-sum test). Plotted are 15, 37, and 9 genes from waves 1–3, respectively. dPRG, delayed PRG.

*(legend continued on next page)*

the best-defined gene modules in inducible systems: primary and secondary response genes (PRGs and SRGs) (Fowler et al., 2011). These gene modules are defined by their requirement for *de novo* translation. PRGs can be induced rapidly and do not require *de novo* translation for their induction, whereas SRGs are induced slowly, require *de novo* translation for their induction, and are regulated by PRG protein products (Fowler et al., 2011; Herschman, 1991). Brief stimulation is sufficient to induce PRGs, but sustained cell signaling pathway activation, which is induced by sustained stimulation, is required to stabilize PRG protein products and induce SRGs (Fowler et al., 2011). In neurons, brief activity could similarly induce only PRGs while sustained activity could be required to induce SRGs. Therefore, defining PRGs and SRGs in neurons and determining their responsiveness to different activity durations could reveal a basic principle underlying the coupling map between activity patterns and gene expression.

In a step toward generating this coupling map, we performed genome-scale comparisons of gene induction in response to neuronal activity patterns of varying duration. We found that different durations of activity induce different sets of genes, allowing us to infer neuronal activity duration from gene expression data. We further reveal that the coupling between activity duration and gene expression is determined in part by MAPK/ERK signaling, enabling future manipulation of the coupling map.

## RESULTS

### Rapid, but Not Delayed, PRGs Are Induced by Brief Activity

We investigated the possibility that different patterns of neuronal activity induce different subsets of ARGs by varying just one aspect of neuronal activity: its duration. We activated neurons briefly (10 s–5 min) or continuously (for up to 6 hr) using three methods of stimulation that allowed us to precisely control the duration of neuronal firing or calcium influx (Figure 1A). We primarily stimulated mouse cultured cortical neurons with KCl-mediated membrane depolarization and assessed the resulting gene induction using either total RNA-seq, which allowed us to assess both mRNA and pre-mRNA transcription (Gaidatzis et al., 2015; Gray et al., 2014), or targeted sequencing of 251 ARG mRNAs (ARG-seq), which allowed us to reduce the number of reads needed per experiment (Table S1; Figure S1A; see STAR Methods).

We first used ARG-seq to characterize the gene induction in response to sustained activity. We found that sustained activity induces 173 ARGs, 114 of which also show significant induction in at least one of three *in vivo* studies (Cho et al., 2016; Lacar et al., 2016; Spiegel et al., 2014) (significant overlap,  $p = 0.0002$ , Fisher's exact test). We observed that these 173 ARGs are induced in two waves, as expected (Flavell

and Greenberg, 2008): a rapid wave that includes 19 genes and a delayed wave that includes 154 genes (Figures 1B and 1C; Figures S1C–S1E, see STAR Methods for details of classification). We hypothesized that the first wave corresponds to the *de novo* translation-independent PRGs and the second to SRGs, which require PRG protein products for their induction. Indeed, after defining PRGs and SRGs based on their requirement for *de novo* translation, we found that the first wave of gene induction is entirely comprised of PRGs (Figure 1B; Figure S1B). However, the second wave includes both PRGs and SRGs, similar to findings in human cancer cell lines and macrophages (Ramirez-Carrozzi et al., 2006; Tullai et al., 2007). Thus, neurons also induce two kinetically distinct classes of PRGs: rapid PRGs (rPRGs) and delayed PRGs (dPRGs). A finer-grained time course using high-throughput qPCR revealed that dPRGs are actually induced earlier than SRGs, suggesting that rPRGs, dPRGs, and SRGs represent three temporally distinct waves of transcription (Figure 1C; Figure S1G; Table S3).

We next measured gene induction in response to brief, KCl-mediated activity using ARG-seq. Remarkably, rPRGs comprise 14 of the 15 genes significantly induced by brief activity (FDR < 0.05, mean fold change > 1.5) (Figures 1B and 1C; Figures S1D and S1G). Pre-mRNA expression assessed in total RNA-seq data recapitulated these mature mRNA findings (Figure S1C), suggesting that the differential responsiveness to brief activity between rPRGs and dPRGs is due to transcriptional rather than post-transcriptional mechanisms. The selective induction of rPRGs, but not dPRGs, by brief activity is not specific to KCl-mediated depolarization, as it also occurs following brief (5-min) bicuculline-induced activity in rat primary cortical neurons, as detected by NanoString (Figure S1F; Table S4). rPRGs are also induced by just 10 s of bicuculline-induced synaptic activity (Figure S1H), equivalent to a single burst of firing (Yu et al., 2017). These findings indicate that *de novo* translation independence is not the only requirement for induction in response to brief activity. Instead, rPRGs in neurons may be distinguished from dPRGs by transcriptional mechanisms that allow them to respond both rapidly and to brief activity.

To confirm that rPRGs, but not dPRGs, are induced in response to brief activity *in vivo*, we assessed gene induction in the visual cortex in response to a visual stimulus consisting of bright, flashing lights (Figure 1D). Using photometry-based *in vivo* recordings of calcium activity, we first confirmed that neuronal activity in primary visual cortex increases with the onset of each flash of light, even for repeated flashes presented for several hours (Figures S2A and S2B). We assessed mRNA induction using qPCR with primers for four rPRGs and eight dPRGs, as classified using our *in vitro* data. The rPRGs are all induced rapidly and in response to 1 min of visual stimulation, consistent with *in vitro* findings (Figure 1E; Figure S2C). Most

(D) Experimental system for comparing the duration of neuronal activation in the visual cortex *in vivo*. Mice were dark housed for 3 days prior to visual stimulation consisting of lights flashing in a repeated pattern: 60 s on, 20 s off.

(E) Gene induction in the visual cortex following visual stimulation as measured by qPCR. Colored points are means of  $n = 3$  biological replicates. Gray points are values from individual biological replicates. Gene categories defined as in (B). \*significant induction compared to 0 hr time point,  $p < 0.05$  unpaired, two-sided t test, fold induction > 1.5.

See also Figures S1 and S2 and Tables S2 and S3.

of the dPRGs (7/8) have delayed induction kinetics and no induction in response to 1 min of stimulation, again consistent with our *in vitro* results. The exception, *Nr4a3*, is induced rapidly and by brief activity, thus behaving as a rPRG *in vitro* but a dPRG *in vivo*. The concordance between our *in vitro* and *in vivo* results suggests that activity duration is coupled to gene expression similarly in primary cortical neurons and in the cortex.

Our finding that dPRGs are induced in response to sustained, but not brief, activity suggests that there is a minimum activity duration required to induce dPRGs. To determine whether this minimum is the same for every dPRG, we assessed PRG expression in response to an intermediate duration of visual stimulation. This intermediate (7-min) stimulus is sufficient to induce only a subset (five) of the seven dPRGs (Figure 1E; Figure S2C), indicating that different dPRGs have different minimum activity duration thresholds. The observation that there are three distinct ARG induction profiles for 1-min, 7-min, and sustained activity suggests that ARG induction has a graded response to the duration of activity and hints at the potential complexity of the coupling between activity pattern and ARG induction.

We next investigated whether the genes in each of the three waves of ARG induction differ in their known or annotated gene function (Table S5). Most (17/19) rPRGs that we identified in mouse cortical neurons are directly or indirectly involved in regulating transcription. rPRGs are also more likely than dPRGs or SRGs to be stimulus-induced in macrophages ( $p = 0.0004$ , Fisher's exact test) (Escoubet-Lozach et al., 2011) and human cancer cell lines ( $p = 0.0001$ , Fisher's exact test) (Tullai et al., 2007), consistent with the idea that transcription factors are reused in many cell types. Therefore, most (112/114) of the effector (i.e., non-transcription-regulating) ARGs, which are thought to orchestrate transcription-dependent neuronal plasticity, are dPRGs or SRGs. A major exception is the rPRG effector gene *Arc* (Shepherd and Bear, 2011). We found that brief activity induces ARC protein in a *de novo* transcription-dependent manner (Figure S1I), consistent with the idea that ARC could mediate the synaptic changes driven by brief activity. These results suggest that any transcription-dependent synaptic changes caused by brief activity are driven by the protein products of only a few genes, including *Arc*.

### Neuronal Activity History Is Encoded in Gene Expression Profiles

Given that brief and sustained activity induce different gene sets, we asked whether we could infer neurons' past activity duration from their ARG expression profiles. Indeed, a nearest-neighbor classifier correctly identified *in vitro* samples as having been stimulated with brief or sustained KCl-mediated depolarization by using normalized expression values from all significantly induced genes or all captured genes, but not constitutively active control genes (Figure 2A). For such classification to be broadly useful, it should be robust to the method of stimulation. We therefore aimed to classify our *in vivo* visual stimulation samples using our *in vitro* KCl-mediated depolarization data as a training set. A classifier using 11 ARGs that have similar expression profiles between *in vitro* and *in vivo* experiments was able to correctly classify 100% of visual cortex samples as having un-

dergone either brief, sustained, or no stimulation (Figure 2B). Thus, the duration of past neuronal activity is indeed encoded in the ARG expression profile, and this information can be used to infer *in vivo* activity histories.

We therefore considered the possibility of using scRNA-seq data to infer the activity histories of thousands of individual neurons in a single experiment (Hrvatin et al., 2018; Hu et al., 2017; Wu et al., 2017). We asked whether we could use scRNA-seq-based detection of ARG expression to identify a population of visual cortex neurons that are activated only briefly in response to sustained visual stimulation. We analyzed published data collected 1 hr after the onset of visual stimulation (Hrvatin et al., 2018). We found that both rPRGs and dPRGs are robustly induced by 1 hr when compared to control mice left in the dark (Figure S3A). We classified neurons that induced rPRGs, but not dPRGs, as having been putatively briefly active ("BRIEF neurons"), whereas those that induced dPRGs were predicted to have had a history of sustained activity ("SUSTAINED neurons") (Figure 2C; Figure S3B). We found that the majority (52%) of neurons were putative SUSTAINED neurons. However, we found a small (13%), but significant, population of putative BRIEF neurons (Figure 2D). The remaining 35% of neurons showed no PRG induction and were therefore classified as putatively inactive. We therefore predict that a subset of neurons in the mouse visual cortex undergoes brief activity in response to sustained visual stimulus.

To determine the identity of these BRIEF neurons, we performed differential gene expression analysis comparing BRIEF and SUSTAINED neurons. We found that the genes expressed significantly more in BRIEF neurons include deep layer (5 and 6) markers such as *Tmem91*, *Gabra5*, *Rprm*, and *Crym*. In contrast, genes with greater expression in SUSTAINED neurons included upper layer (2/3 and 4) markers, such as *Calb1*, *Cux1*, and *Rasgrf2* (fold change  $> 2$ , FDR  $< 0.1$ ; Figure 2E) (layer markers from Hrvatin et al., 2018; Tasic et al., 2016). Impressively, almost all of the genes differentially expressed between BRIEF and SUSTAINED neurons show similar layer-specific trends in expression, suggesting that the major genetic differences between BRIEF and SUSTAINED neurons arise from their layer positions (Figure 2F). We therefore directly asked whether deep layers of the cortex have a greater enrichment for BRIEF neurons than upper layers, using gene-expression-based layer definitions (Hrvatin et al., 2018). We indeed found that deep layers of the cortex have more BRIEF neurons than upper layers, with only deep layers having a statistically significant population of BRIEF neurons (Figure 2G; Figure S3C). We were concerned about being biased toward detecting BRIEF neurons in deep layers if upper layer neurons induce more of the dPRGs on our *in vitro* defined list than deep layers, which is possible given that different layers of cortex induce different dPRGs (Hrvatin et al., 2018). To control for this alternative possibility, we used the scRNA-seq data to define dPRGs for each layer individually and confirmed that we still found an enrichment of BRIEF neurons in deep layers using the layer-specific dPRGs (Figure S3D). This analysis therefore predicts that upon sustained visual stimulation, a population of neurons in layers 5 and 6 of the primary visual cortex exhibits only brief elevations in activity.

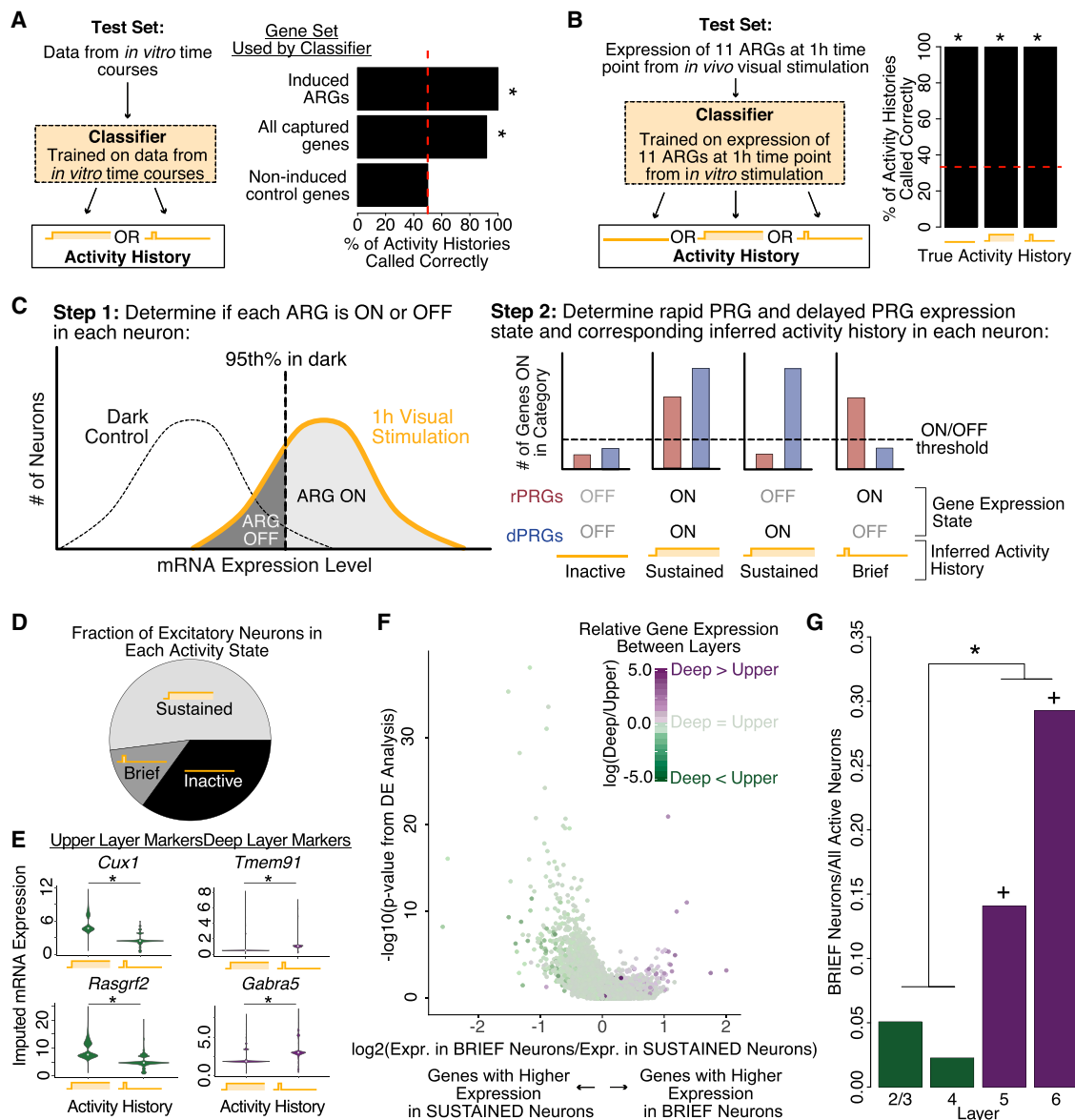


**Figure 2. Neuronal Activity Patterns Can Be Inferred from ARG Expression**

(A) A classifier trained on *in vitro* gene expression data to infer activity histories of 12 *in vitro* samples (6 brief, 6 sustained). The classifier identified test samples as having undergone either brief or sustained activity based on Euclidean distance to training samples. \* $p = 0.007$ , exact binomial test.

(B) A similar (*in vitro* trained) classifier used to infer the activity histories of 12 *in vivo* visual cortex samples (3 brief, 3 sustained, and 6 unstimulated). \* $p < 0.04$ , exact binomial test.

(C) Method for scRNA-seq-based inference of BRIEF and SUSTAINED activity histories of individual visual cortex excitatory neurons from mice exposed to 1 hr of sustained visual stimulation. scRNA-seq data from Hrvatin et al. (2018).

(D) 1 hr of visual stimulation significantly increased the fraction of excitatory neurons with BRIEF and SUSTAINED inferred activity states ( $p < 10^{-15}$ , Fisher's exact test).

(E) Expression of four layer markers in BRIEF and SUSTAINED neurons in scRNA-seq data. Data plotted are imputed mRNA reads after using DECENT (Ye et al., 2017) to account for the presence of technical zeroes. \*FDR < 0.1, rank-sum test.

(F) Differential expression (DE) of all genes (excluding ARGs) in BRIEF compared to SUSTAINED neurons. p value determined using the rank-sum test. Color of the points represent the log of the ratio of gene expression in deep layers (layers 5 and 6) to that in upper layers (layers 2/3 and 4).

(G) Fraction of stimulated neurons in each layer that are BRIEF. \*More BRIEF neurons in deep versus upper layers,  $p < 10^{-15}$ , Fisher's exact test. \*Significant population of brief neurons,  $p < 0.001$  based on a Fisher's exact test comparing the number of rPRG-ON neurons among dPRG-OFF neurons in the stimulated cortex to the number of rPRG-ON neurons in unstimulated cortex.

See also Figure S3.

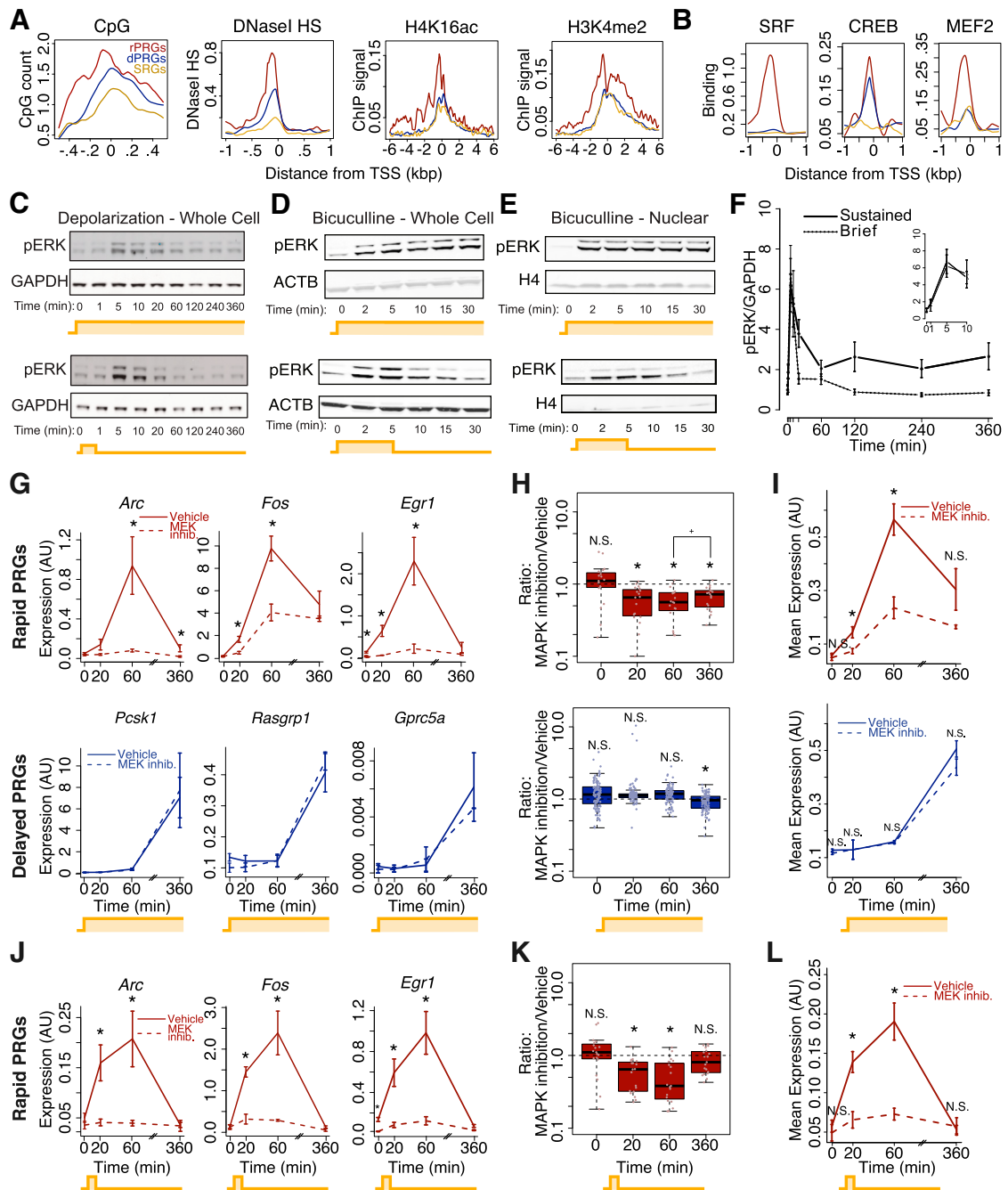


**Figure 3. Requirement for MAPK/ERK Signaling and an Open Chromatin State Distinguish First and Second Waves of Gene Induction**

(A) Chromatin state in unstimulated neurons shown in metaplots of the geometric mean signal for all genes in each category. All measures of chromatin state are significantly different between rPRGs and dPRGs or SRGs ( $p < 0.009$ , rank-sum test on the area under the curves shown). ChIP-seq data are from cultured cortical neurons (Telesse et al., 2015). DNaseI hypersensitivity data are from the 8w cerebrum (ENCODE Project Consortium, 2012).

(B) Transcription factor binding in unstimulated neurons from ChIP-seq shown in metaplots as in (A). SRF and MEF2: significantly different between rPRGs and dPRGs or SRGs; CREB: not significantly different between rPRGs and dPRGs ( $p = 0.2$ ) but is different between rPRGs and SRGs ( $p < 0.009$ , rank-sum test). Data from cultured cortical neurons (Kim et al., 2010; Telesse et al., 2015).

(C) ERK activation kinetics with KCl-mediated depolarization. Representative (1 of  $n = 3$ ) western blot for phosphorylated ERK (pERK). Phosphorylation of ERK paralogs, p44 and p42 (upper and lower bands), is kinetically similar ( $r^2 = 0.97$ , Pearson correlation).

(D) Similar to (C), but rat cortical neurons were treated with sustained or brief bicuculline/4AP. One of  $n = 3\text{--}4$  representative biological replicates is shown.

(E) Same as (D) but from isolated nuclei.

(legend continued on next page)

### Rapid PRG Promoters Are Distinguished by Open, Active Chromatin and the Presence of Pre-bound Transcription Regulators

We next investigated what might enable rPRGs to be induced both rapidly and by brief activity. The faster mRNA induction of rPRGs could be facilitated in part by their shorter gene length compared to dPRGs and SRGs (median ~13 kb shorter; Figure S4A). However, we found that rPRG first exons are induced before those of dPRGs or SRGs (Figure S4B), indicating that rPRG promoters are also activated more rapidly. We hypothesized that rPRG promoters might be primed for faster promoter activation due to an open chromatin state prior to stimulation. To assess this hypothesis, we evaluated three marks of open chromatin: high DNaseI hypersensitivity (data from ENCODE Project Consortium, 2012), high CpG (and GC) content, and high levels of active chromatin marks, including H4K16ac, H3K4me2, and H3K27ac (data from Kim et al., 2010; Telese et al., 2015). We found that by all three of these criteria, unstimulated rPRG promoters have more open chromatin than unstimulated dPRG or SRG promoters (Figure 3A; Figures S4C and S4D). Importantly, the histone acetylation signals extend across a wider promoter-proximal region and are more bimodal at rPRG promoters, indicative of reduced nucleosome occupancy at or near transcription start sites prior to stimulation (Figure 3A; Figures S4C and S4D). These differences in average DNase hypersensitivity and histone marks could be due to the greater number of neuronal and non-neuronal brain cell types that induce rPRGs compared to dPRGs and SRGs (Hrvatin et al., 2018) rather than to differences in chromatin accessibility in the neurons that actually induce each class. However, the observation that rPRGs have more open chromatin than dPRGs and SRGs in homogeneous non-neuronal cell populations (Hargreaves et al., 2009; Ramirez-Carrozzi et al., 2009, 2006) leads us to favor the idea that rPRG promoters in neurons are also distinguished by a relatively open chromatin state, potentially poising them for rapid activation in response to brief activity.

The open chromatin state at rPRG promoters in unstimulated neurons prompted us to ask whether these promoters might be selectively pre-bound to transcriptional regulators prior to neuronal activation. We found that RNA polymerase 2 (Pol2) occupancy in unstimulated neurons is higher at the promoters of rPRGs and constitutively active genes compared to dPRGs and SRGs (Figures S4F and S7E) despite the finding

that rPRGs, dPRGs, and SRGs have similar levels of transcription in unstimulated neurons (Figure S4G). Furthermore, we found greater binding of the neuronal activity-regulated transcription factors SRF and MEF2, as well as the Mediator subunits MED23 and MED1 (Figure 3B; Figure S4E), at rPRG promoters compared to dPRG or SRG promoters in unstimulated neurons (data from Kim et al., 2010; Telese et al., 2015). In contrast, the transcription factor CREB is pre-bound to a similar extent to rPRG and dPRG promoters but is not pre-bound to SRG promoters (Figure 3B; Figure S4E). Interestingly, the NCoR repressor complex also binds preferentially to rPRG promoters compared to dPRG or SRG promoters (Figure S4H) and could prevent them from being transcribed despite their open state. These data suggest that in addition to an open chromatin state, pre-binding of transcriptional activators may uniquely poise rPRGs for rapid induction in unstimulated neurons.

### The MAPK/ERK Pathway Is Required for the First Wave of Gene Induction

We next asked whether rPRGs are targeted by a rapidly activated signaling pathway that endows them with the ability to respond quickly and to brief activity. In evaluating this possibility, we compared rPRGs and dPRGs but excluded SRGs to eliminate the confounding possibility of altered PRG induction affecting SRG induction. We first hypothesized that the CaMKIV pathway might mediate rPRG induction due to its role in rapid phosphorylation of the transcription factor CREB (Hardingham et al., 2001; Wu et al., 2001b). Using immunocytochemistry, we observed phospho-CaMKIV in the nucleus within just 5 min of membrane depolarization, indicating rapid pathway activation (Figure S5A). However, when we blocked CaMKIV phosphorylation using an inhibitor for the upstream kinase CaMKK (Figure S5A), we found no effect on induction of rPRGs or dPRGs in response to either brief or sustained activity despite a small effect on ARG expression in unstimulated neurons (Figures S5B and S5C; Table S3). Therefore, the rapid induction and sensitivity to brief activity of rPRGs is not explained by a dependence on CaMKIV signaling.

We next asked whether another canonical neuronal signaling pathway, the MAPK/ERK pathway (Thomas and Huganir, 2004), is activated rapidly and in response to brief activity, which would be consistent with selective regulation of rPRGs. We assessed MAPK/ERK pathway activation by western blotting

(F) Quantification of (C), n = 3 biological replicates. The inset is a magnified version of the first 10 min. pERK induction at its peak (5 min) is not different between brief and sustained stimulus ( $p = 0.3$ , paired, two-sided t test). Error bars represent  $\pm$ SEM.

(G) rPRG, but not dPRG, induction in response to sustained activity is dependent on MAPK/ERK. ARG-seq-based gene expression of three representative rPRGs and three representative dPRGs following sustained KCl depolarization of mouse neurons with and without 10  $\mu$ M of the MEK inhibitor U0126. n = 3–7 biological replicates. Error bars are  $\pm$ SEM. \* $p < 0.01$ , rank-sum test.

(H) Data from the same experiment as (G) showing all ARGs. \*significantly different from 1,  $p < 0.01$ , rank-sum test; \* $p = 0.02$ , rank-sum test. Expression of rPRGs is more affected by MEK inhibition than expression of dPRGs ( $p = 0.002$ ; rank-sum test on 17 rPRGs versus 110 dPRGs using the mean for each gene across n = 3–7 biological replicates at its most induced time point).

(I) Data the same as in (H) but showing the geometric mean of gene expression. Error bars are  $\pm$ SEM from each of n = 3–7 biological replicates of all genes in the category. \* $p < 0.03$ , rank-sum test.

(J) rPRG, but not dPRG, induction in response to brief activity is dependent on MAPK/ERK. Same as (G), top row, but with 1 min KCl depolarization.

(K) Same as (H), top row, but with 1 min KCl depolarization.

(L) Same as (I), top row, but with 1 min KCl depolarization.

See also Figures S4–S6 and Table S2.

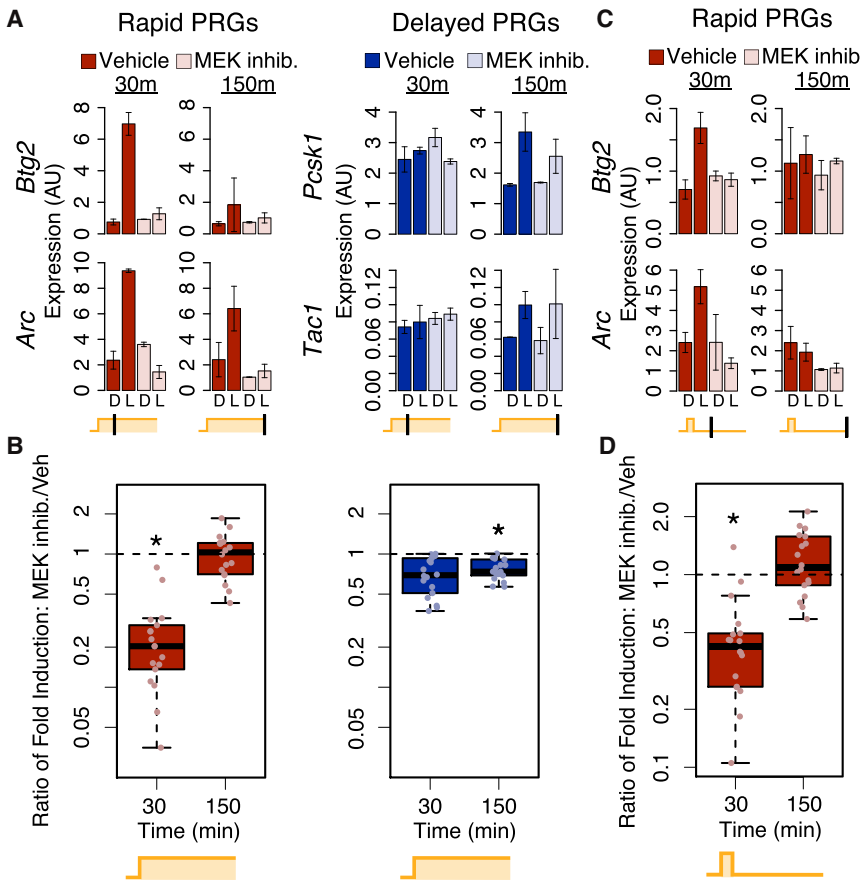


**Figure 4. MAPK/ERK Is Required for the First Wave, but Not the Second Wave, of Gene Induction In Vivo**

(A) Visual-stimulus-mediated gene induction of representative genes in the visual cortex upon sustained stimulation in mice injected intraperitoneally with corn oil vehicle or the MEK inhibitor SL327 (100 mg/kg), based on ARG-seq. D, dark, no visual stimulation; L, light, with visual stimulation. Error bars are 95% confidence intervals across  $n = 2\text{--}3$  mice.

(B) Same experiment as (A), but showing all rPRGs or dPRGs detected by ARG-seq from  $n = 2\text{--}3$  biological replicates. \* $p < 0.01$  from rank-sum test, significant difference from 1. Induction of rPRGs is more affected by MEK inhibition than induction of dPRGs ( $p = 0.02$ ; rank-sum test, 16 rPRGs versus 14 dPRGs using the mean for each gene at its most induced time point across  $n = 2\text{--}3$  biological replicates).

(C) Same as (A) but with brief visual stimulation.

(D) Same as (B) but with brief visual stimulation.

See also Figure S6 and Table S2.

for the pathway's terminal kinase phospho-ERK (pERK). In response to both brief and sustained activity, pERK levels reach the same peak magnitude by 5 min after the start of activity (Figures 3C, 3D, and 3F), suggesting that the MAPK/ERK pathway is rapidly and fully activated by brief activity. Because pERK can activate transcription via phosphorylation of nuclear proteins (Thomas and Huganir, 2004), we confirmed that the MAPK/ERK target transcription factor Elk-1 is phosphorylated rapidly and MAPK/ERK dependently in response to sustained depolarization (Figure S6A). In further support that the MAPK/ERK pathway signals rapidly to the nucleus, we detected increased pERK in the nucleus by 2 min following both brief and sustained neuronal activity (Figure 3E). Interestingly, upon brief stimulation, ERK activity remains elevated for at least 10 min after the removal of stimulus, which is more than sufficient time for activation of rPRG transcription.

We therefore hypothesized that the MAPK/ERK pathway is required for rPRG induction. To test this hypothesis, we measured ARG induction using ARG-seq in the presence of MAPK/ERK pathway inhibition (Figure S6B) using the potent and highly specific allosteric MEK inhibitor U0126 (Favata et al., 1998). We found that MEK inhibition dramatically blunts induction of rPRGs, but not dPRGs, in response to sustained activity (Figures 3G–3I). 95% of rPRGs but only 17% of dPRGs are sensitive to MEK inhibition (based on >40% decrease in maximum expression; Figure 3H). We also confirmed that MEK

inhibition blocks induction of rPRG, but not dPRG, pre-mRNAs, suggesting that the MAPK/ERK pathway acts at the level of transcription (Figure S6C). This blunting of gene induction is unlikely to be due to off-target effects of U0126, since the MEK inhibitor PD184352 and the ERK inhibitor 11e have similar effects (Figures S6G and S6H). Most rPRGs are partially

induced in the presence of MEK inhibition, but with delayed kinetics, indicating that MAPK/ERK activity is most important for the early stages of gene induction (Figures S6E and S6F).

We next asked whether MAPK/ERK signaling is also required for gene induction in response to brief activity. Impressively, MEK inhibition substantially decreases mRNA and pre-mRNA induction in response to brief activity (Figures 3J–3L; Figures S6D and S6I), blunting mRNA induction of all but one of the induced rPRGs. Again, we observed similar results using the ERK inhibitor 11e (Figure S6G). Therefore, the MAPK/ERK pathway is required for rapid ARG induction and induction in response to brief activity, thus establishing the first wave of ARG induction *in vitro*.

We next investigated whether the MAPK/ERK pathway is required for rapid gene induction *in vivo*. We exposed dark-housed mice to brief (1-min) or sustained (up to 2.5-hr) visual stimulation, consisting of turning on the room lights, in the presence or absence of MEK inhibition (Figure S6J). ARG-seq of the visual cortex revealed that MEK inhibition has a larger effect on rPRG compared to dPRG expression in cortices from mice exposed to sustained visual stimulation (Figures 4A and 4B), and it blocks nearly all ARG induction in mice exposed to brief visual stimulation (Figures 4C and 4D). Most of the ARG induction we observed appears to be due to the visual stimulation itself rather than stress from the lights or handling, as we did not observe induction of the rPRG *Fos* in the prefrontal cortex of

mice exposed to visual stimulus (Figure S6K). We also confirmed that for the room-light visual stimulation used for this experiment, brief stimulation induces rPRGs better than dPRGs and SRGs (Figure S6L). We therefore conclude that, both *in vivo* and *in vitro*, the MAPK/ERK pathway is a fast pathway necessary for rapid ARG induction and induction in response to brief activity.

### The MAPK/ERK Pathway Mediates Fast Pol2 Recruitment to Rapid PRG Promoters

We next sought to understand how the MAPK/ERK pathway mediates rapid induction of rPRG promoters. Because ARG induction is accompanied by Pol2 recruitment to ARG promoters within the first 2 hr of activity (Kim et al., 2010), we hypothesized that the rapidity of rPRG induction could be mediated by fast, MAPK/ERK-dependent Pol2 recruitment. Indeed, using Pol2 chromatin immunoprecipitation sequencing (ChIP-seq), we observed a rapid increase in Pol2 occupancy at rPRG promoters by 1 to 10 min of activity (Figures 5A and 5B; Figures S7A, S7B, and S7G). We also found that pharmacological blockade of new transcription initiation completely abolishes rPRG mRNA induction (Figure S7F), suggesting that initiation of transcription by newly recruited Pol2 is essential for rPRG induction. To ask whether MAPK/ERK signaling is required for the rapid recruitment of Pol2 to rPRG promoters, we performed Pol2 ChIP-seq in a time course of neuronal stimulation in the presence and absence of MEK inhibition. MEK inhibition reduces Pol2 occupancy at rPRG promoters at 10 and 30 min of activity (Figures 5A–5C; Figures S7A and S7B), indicating that MAPK/ERK signaling is required for rapid recruitment of Pol2 to these promoters. However, MEK inhibition has no effect at later time points, suggesting that other pathways mediate slower Pol2 recruitment to rPRG promoters. Because pre-bound, paused Pol2 may facilitate faster recruitment of Pol2 by maintaining an open chromatin state (Gilchrist et al., 2010), we next asked whether MAPK/ERK signaling might enable rapid Pol2 recruitment by mediating the pre-binding and pausing of Pol2 at rPRG promoters in unstimulated neurons (Saha et al., 2011). We found that MEK inhibition does not change the Pol2 occupancy at rPRG promoters in unstimulated neurons (Figure 5A; Figure S7A), indicating that MAPK/ERK signaling is required specifically for rapid, activity-dependent Pol2 recruitment.

We next assessed the effect of MAPK/ERK signaling on Pol2 recruitment to dPRG promoters. Surprisingly, despite the slow transcriptional induction of dPRGs, we observed recruitment of Pol2 to many of their promoters by 10 min of neuronal activation (Figures 5D and 5E; Figures S7C and S7D). However, in contrast to rPRGs, recruitment of Pol2 to dPRG promoters is not affected by MEK inhibition at early or late time points either for the full set of dPRGs (Figures 5D–5F; Figures S7C and S7D) or a restricted set with greater Pol2 occupancy ( $FDR > 0.01$ , rank-sum test, see STAR Methods). These results are consistent with a model in which MAPK/ERK signaling is required for rapid Pol2 recruitment to rPRG promoters, which are primed by pre-bound transcriptional machinery, but not for recruitment to dPRG promoters, which may require chromatin remodeling.

### The MAPK/ERK Pathway Is Required for eRNA Transcription, but Not H3K27 Acetylation, at Rapid Enhancers

Pol2 could be recruited to the promoters of rPRGs in a MAPK/ERK-dependent manner via delivery from genomic enhancers (Szutorisz et al., 2005). We therefore asked whether enhancer activation might be dependent on MAPK/ERK signaling using H3K27 acetylation (H3K27ac) as a proxy for enhancer activity (Creighton et al., 2010; Rada-Iglesias et al., 2011). We performed H3K27ac ChIP-seq throughout a time course of neuronal activation and analyzed H3K27ac levels at 940 putative ARG enhancers. We hypothesized that enhancers near rPRGs would have rapid, activity-dependent activation and require MAPK/ERK signaling whereas enhancers near dPRGs would be activated slowly and be MAPK/ERK independent. Surprisingly, most activity-regulated enhancers rapidly gain H3K27ac within 10 min of activity regardless of the kinetics of their nearby promoters (Figures 6A–6C). Furthermore, accumulation of H3K27ac does not require MAPK/ERK signaling, as MEK inhibition has no effect on activity-dependent H3K27ac at these enhancers, including those near MEK-dependent rPRGs (Figure 6D; Figure S8A). Thus, H3K27ac neither is MAPK/ERK dependent nor kinetically distinguishes enhancers near rPRGs versus dPRGs.

We next assessed another proxy of enhancer activity, enhancer RNA (eRNA) transcription (Kim et al., 2010). Surprisingly, total RNA-seq revealed that eRNA is induced more rapidly at enhancers near rPRGs than at those near dPRGs, thus mirroring mRNA expression kinetics more closely than H3K27ac (Figure 6E). Furthermore, in contrast to our finding that H3K27ac is unaffected by MEK inhibition, MEK inhibition attenuates eRNA induction at enhancers near rPRGs (Figure 6F; Figure S8A). These results indicate that rPRGs are distinguished by their proximity to rapidly activated enhancers whose eRNA induction, but not H3K27ac, is MAPK/ERK dependent.

We next asked whether the rapidity of eRNA induction near rPRGs is inherent to the enhancers themselves or simply a byproduct of activation of nearby promoters. We predicted that if enhancer activation properties are inherent to the enhancers, we should observe a subset of enhancers whose kinetics and sensitivity to brief activity differ from their nearby promoters. To test this prediction, we needed to assess enhancers individually rather than in groups based on the kinetics of nearby promoters (as above). We therefore developed (Figures 7A and 7B; Table S1) and validated (Figure S8B) a targeted capture method, eRNA-seq, to enrich RNA-seq libraries for eRNAs by about 500-fold. We then identified and classified activity-regulated enhancers as rapid or delayed based on the kinetics of their eRNA induction (Figure 7C). While most activity-regulated enhancers near rPRG promoters are rapid enhancers, a minority (21%) are delayed enhancers (Figures 7D and 7E). Moreover, 50% of activity-regulated enhancers near dPRGs are rapid and 50% are delayed enhancers (Figure 7D), supporting the idea that enhancer activation kinetics are inherent to enhancers rather than nearby promoters. In further support of this idea, we found that rapid enhancers are more sensitive to brief activity than delayed enhancers (Figure 7H) even when considering only those enhancers near dPRGs ( $p < 10^{-4}$ , rank-sum test, see STAR Methods). This dissociation between the kinetics

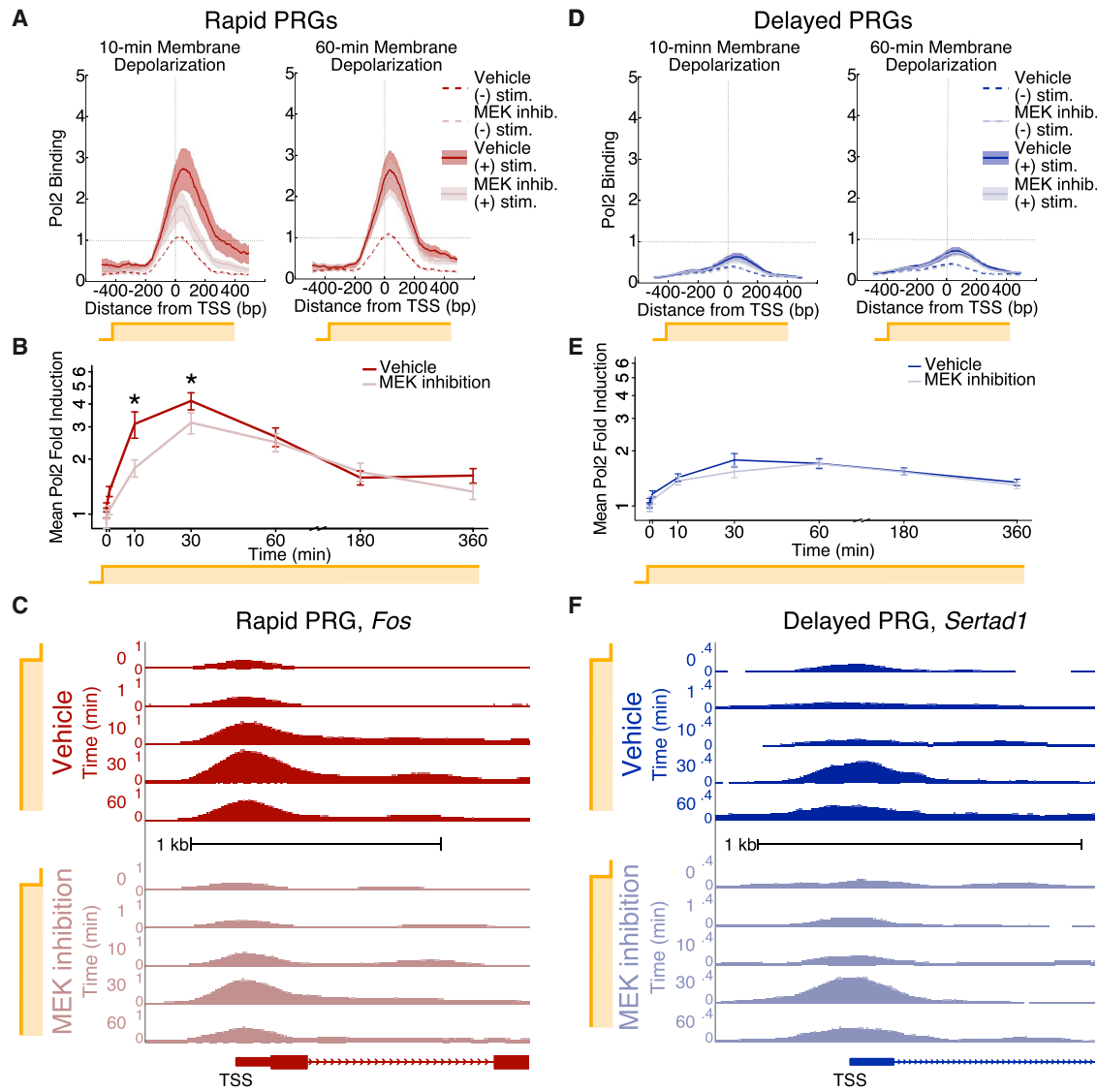


**Figure 5. MAPK/ERK Mediates Fast Recruitment of Pol2 to Rapid PRG Promoters**

(A) RNA polymerase 2 (Pol2) binding (ChIP-seq) at the promoters of rPRGs. Lines represent the mean and shading the SEM across loci. Data shown are from  $n = 1$  of 2 biological replicates. Pol2 binding to rPRG promoters is blunted by MEK inhibition (see B). The KCl-dependent fold increase in mean Pol2 density ( $-300$  bp to  $+300$  bp) is significant under both vehicle and MEK inhibitor treatments (FDR  $< 0.001$  in each of two biological replicates, paired rank-sum test). MEK inhibition does not affect Pol2 occupancy in unstimulated neurons (FDR  $> 0.05$  in each of two biological replicates, paired rank-sum test).

(B) ChIP-seq-based time course of fold change in Pol2 occupancy at rPRG promoters ( $-300$  bp to  $+300$  bp). Shown are mean fold change values across genes, with  $\pm$ SEM error bars. \*FDR  $< 0.01$  in each of two replicates, paired rank-sum test on fold change values.

(C) Pol2 binding at the promoter of the representative rPRG *Fos* upon sustained neuronal activation. Data normalized prior to visualization.

(D) Plotting and statistics same as (A) but showing dPRG promoters.

(E) Plotting and statistics as in (B) but showing dPRG promoters.

(F) Plotting as in (C) but showing representative dPRG *Sertad1*.

See also Figure S7 and Table S7.

and brief activity sensitivity of a subset of enhancers and their nearby promoters supports the idea that enhancer activation is not merely a byproduct of transcription at the promoter.

After identifying individual enhancers as inherently rapidly activated, we asked whether rapid eRNA induction at rapid enhancers might be mediated by an open chromatin state and sensitivity to MAPK/ERK signaling, similar to mRNA induction

from rPRG promoters. Indeed, compared to delayed enhancers, we found that rapid enhancers have significantly elevated CpG content. They also have more open, active chromatin in unstimulated neurons as evidenced by higher DNase hypersensitivity, greater binding of the transcription activators SRF, MEF2, and Mediator, and greater binding of the transcriptional repressor NCoR (Figures 7F and 7G; Figures S8C and S8D). However,

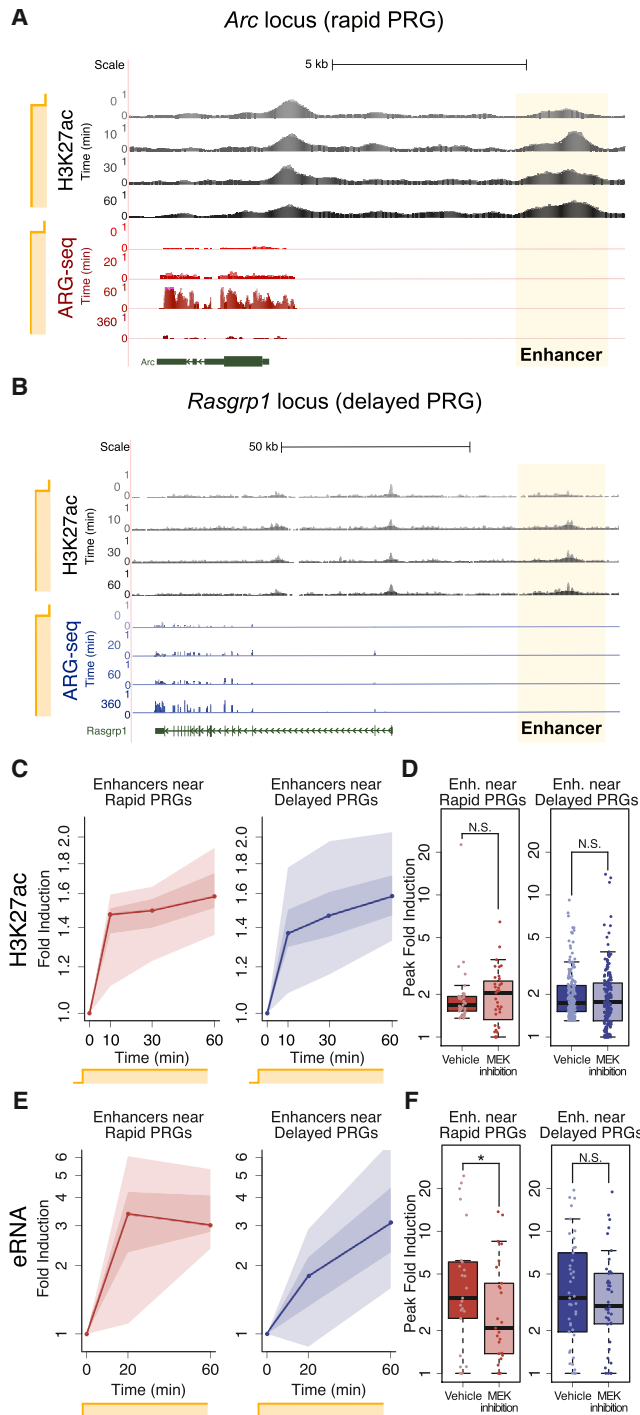


**Figure 6. MAPK/ERK Is Required for Rapid eRNA Induction, but Not H3K27 Acetylation, at Enhancers**

(A) H3K27ac accumulation (ChIP-seq) at the rPRG *Arc* locus upon sustained KCl depolarization. The gene expression of *Arc* based on ARG-seq is shown for comparison. Data normalized by read depth prior to visualization.

(B) Same as (A) but for the dPRG *Rasgrp1*.

(C) H3K27ac accumulation (ChIP-seq) at enhancers upon sustained KCl depolarization. Plotted are means from  $n = 2$  biological replicates. Lines represent the median across enhancers, dark shading the two middle deciles, and light shading the upper and lower quartiles. The increase from 0 to 10 min is

unlike rPRG promoters, rapid enhancers show little binding of Pol2 in unstimulated neurons (Figure S8C). The more active chromatin state at rapid enhancers appears to be intrinsic to the enhancers themselves rather than an indirect effect of their associated promoters, since a comparison of just those rapid and delayed enhancers near dPRGs revealed the same differences in CpG content, active chromatin marks, and transcription factor pre-binding in unstimulated neurons ( $p < 0.01$ , rank-sum test, see STAR Methods). Using eRNA-seq in the presence of a MEK inhibitor, we also found that rapid enhancers are more sensitive to MAPK/ERK inhibition than delayed enhancers (Figures 7E and 7I; Figure S8E). In the case of at least one enhancer, Fos “e5” (Joo et al., 2016), MAPK/ERK-dependent enhancer activation is required for activity-dependent promoter activation based on a luciferase reporter assay (Figure 7J). These results indicate that rapid enhancers are primed for rapid MAPK/ERK-dependent activation whether they are near first- or second-wave genes.

## DISCUSSION

Using genome-scale technology, we demonstrate that a neuron’s activity pattern is encoded in its gene expression profile. Furthermore, we uncover a principle underlying the coupling map that links activity pattern to gene expression: the duration of neuronal activity has a logical relationship to three temporally and mechanistically distinct waves of gene induction. These three waves of gene induction include rPRGs, dPRGs, and SRGs, which are all induced by sustained neuronal activity. In contrast, brief activity induces only the first of these waves, rPRGs, which are uniquely dependent on MAPK/ERK signaling for their induction (Figure 8). Abolishing MAPK/ERK signaling not only alters the multi-wave structure of the ARG response by blunting and delaying rPRG induction, but it also abolishes rPRG induction in response to brief activity. In this way, MAPK/ERK both establishes the multi-wave structure of ARG transcription and enables activity-duration-specific gene induction. This shared mechanism suggests that a biological advantage of the multi-wave structure of ARG induction is to enable different activity patterns to induce different subsets of genes.

## MAPK/ERK Establishes the First Wave of Gene Induction

We identify the MAPK/ERK pathway as a key determinant of the first wave of neuronal ARG induction, enabling first-wave genes to respond rapidly and to brief activity. However, our results suggest that other pathways must establish later waves of ARG

significant for both enhancers near rPRGs and those near dPRGs ( $p < 0.00001$ , rank-sum test).

(D) H3K27ac accumulation at enhancers near rPRGs and dPRGs is not significantly affected by MEK inhibition ( $p > 0.2$ , rank-sum test). Data as in (C). The y axis shows the induction at each enhancer’s most-induced time point (10, 30, or 60 min) in each condition.

(E) eRNA induction (total RNA-seq) upon neuronal activation. Plotted as in (C).

(F) MEK inhibition blocks eRNA induction at enhancers near rPRGs, but not dPRGs. Plotting as in (D), except showing the maximum eRNA induction at 20 or 60 min. \* $p = 0.01$ , rank-sum test, using means for each enhancer from  $n = 2$  biological replicates; N.S.,  $p > 0.05$ .

See also Figure S8 and Tables S2 and S8.

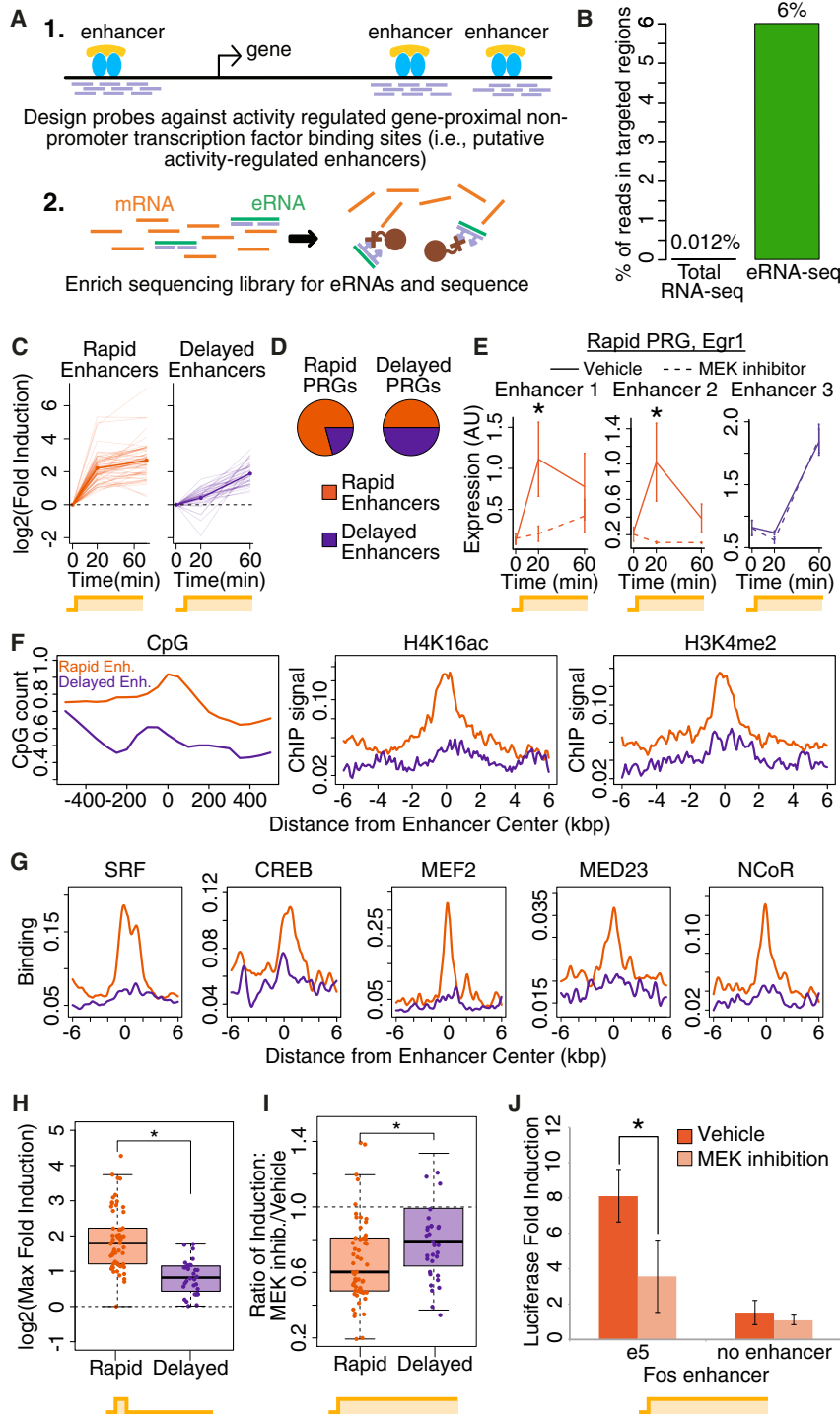


**Figure 7. eRNA-Seq Enables eRNA Quantification at Individual Enhancers, Revealing Rapid and Delayed Enhancers**

(A) eRNA-seq methodology.

(B) Reads in target enhancers: eRNA-seq versus total RNA-seq.

(C) eRNA-seq-based eRNA expression at significantly induced (FDR < 0.05) rapid and delayed enhancers upon sustained activation. Rapid enhancers are significantly induced by 20 min and delayed enhancers only by 60 min. Light lines are means for individual enhancers from  $n = 4$  biological replicates, and heavy lines are the geometric means for all enhancers shown.

(D) rPRGs compared to dPRGs are enriched for the presence of nearby rapid enhancers ( $p = 0.02$ , Fisher's exact test), but there are also rapid enhancers near dPRGs.

(E) eRNA-seq-based eRNA expression at three enhancers near the rPRG *Egr1* revealing two rapid and one delayed enhancer. \* $p < 0.05$ , paired rank-sum test. Error bars are means  $\pm$  SEM.

(F) Indicators of open chromatin prior to stimulation at rapid versus delayed enhancers, with metaplots showing the geometric mean of all enhancers in each class. All are significantly different between rapid and delayed enhancers ( $p < 10^{-7}$ , rank-sum test using area under the curve). ChIP-seq data from cultured cortical neurons (Telese et al., 2015).

(G) Binding of transcription factors, the mediator subunit MED23, and NCoR at rapid versus delayed enhancers prior to stimulation, shown as in (F). All are significantly different between rapid and delayed enhancers ( $p < 10^{-4}$ , rank-sum test on area under the curve). ChIP-seq data from cultured cortical neurons (Kim et al., 2010; Telese et al., 2015).

(H) Rapid enhancers show greater induction in response to brief activity than delayed enhancers based on eRNA-seq ( $p < 10^{-9}$ , rank-sum test). The y axis shows the mean fold induction from  $n = 4$  biological replicates for each enhancer at its most-induced time point (20 or 60 min).

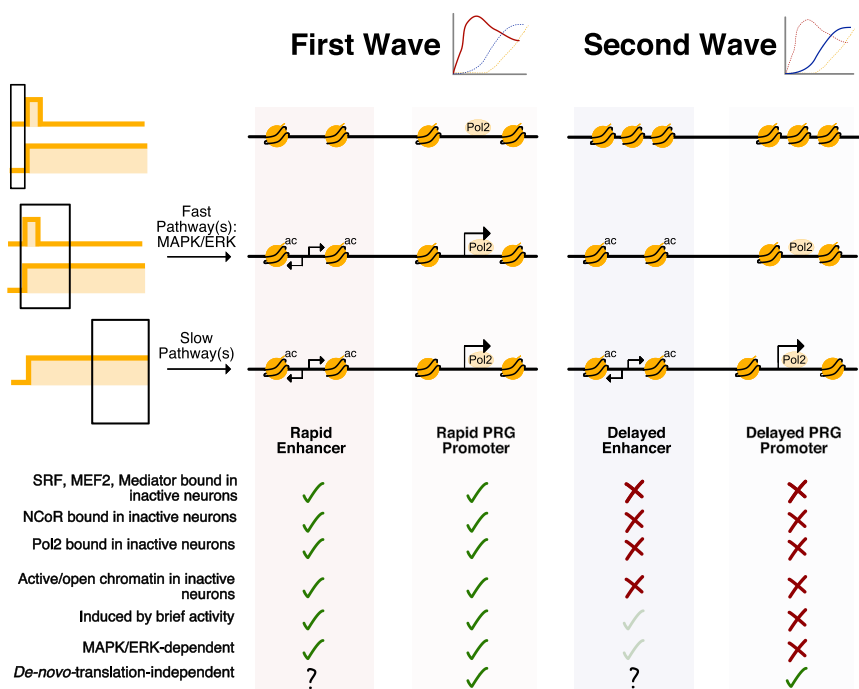
(I) Rapid enhancers are more MAPK/ERK-dependent than delayed enhancers, based on eRNA-seq ( $p = 0.006$ , rank-sum test, using means for each enhancer from  $n = 4$  biological replicates). For each class of enhancers, the earliest time point at which that class exhibits significant eRNA induction is shown (20 min for rapid and 60 min for delayed enhancers). The y axis shows the KCl-dependent fold induction with MEK inhibition divided by the same fold induction with vehicle treatment only (i.e., ratio of fold inductions).

(J) Effect of MEK inhibition on the enhancer function of the *Fos* enhancer e5 using a luciferase reporter assay in which the enhancer drives transcription from a minimal *Fos* promoter. \* $p < 0.03$  from t test based on  $n = 3$  biological replicates. Error bars represent  $\pm$ SEM.

See also Figure S8 and Table S2.

induction. In contrast to this idea that multiple different pathways each regulate their own subset of genes, in PC12 cells, the MAPK/ERK pathway itself mediates two different cellular outcomes depending on the duration of MAPK/ERK activation (Gotoh et al.,

1990; Marshall, 1995; Santos et al., 2007). Our finding that the MAPK/ERK pathway is a fast pathway for activating ARG induction also differs from previous studies that suggest it could be a relatively slow regulator of transcription, including those showing

**Figure 8. Distinguishing Features of First-Wave Genes and Second-Wave Genes**

rPRGs are distinguished by dependence on MAPK/ERK signaling, proximity to rapid enhancers, and an open chromatin state. Light green check marks indicate partial effects.

that it is slow to phosphorylate the transcription factor CREB (Hardingham et al., 2001; Murphy et al., 1994; Toettcher et al., 2013; Wu et al., 2001b). Slow MAPK/ERK-dependent phosphorylation of CREB could be important for regulating SRGs, especially given the persistence of phospho-ERK in response to sustained stimulation. Despite its slow phosphorylation of CREB, others have found that the MAPK/ERK pathway can be rapidly activated in the nucleus in response to brief stimulation (Dudek and Fields, 2001; Zhai et al., 2013) and is required for induction of several genes that we can now classify as rPRGs (Davis et al., 2000; Eriksson et al., 2007; Zheng et al., 2009).

There are at least two ways that MAPK/ERK could specify which genes are included in the first wave. In a passive model, rPRG promoters could be uniquely sensitive to MAPK/ERK signaling solely due to their open chromatin state in inactive neurons. This open chromatin state could prime rPRG promoters to be activated by MAPK/ERK within the first few minutes following neuronal activation, when MAPK/ERK is most active. Our study (Figure S7E) and previous work (Saha et al., 2011) suggest that this open chromatin state may be maintained in inactive neurons by the paused Pol2 found at rPRG promoters prior to neuronal activation. This function for Pol2 is consistent with the current view of the function of paused Pol2 generally (Gilchrist et al., 2010) as well as our finding that the paused Pol2 is insufficient for appreciable gene induction in the absence of new Pol2 recruitment and initiation. In an active model of how MAPK/ERK specifies first-wave genes, MAPK/ERK signaling could activate rPRGs due to specific binding of MAPK/ERK-dependent transcriptional activators, including SRF (Treisman, 1996). SRF is required *in vivo* for the transcription of rPRGs (Ramanan et al., 2005) and often acts in concert with Elk-1, which is directly phosphorylated by MAPK/ERK (Figure S6A; Marais et al., 1993; Sgambato et al., 1998; Xia et al., 1996). Elk-1 facilitates Pol2

recruitment via interactions with the Mediator subunit MED23 (Allen and Taatjes, 2015; Wang et al., 2005). We present correlative evidence that rPRGs may be regulated by SRF, Elk-1, MEF2, and MED23 and by activation of nearby rapid enhancers, but further work is required to causally link these mechanisms to rPRG induction.

### Separable Mechanisms of Enhancer Activation Revealed by MAPK/ERK

Surprisingly, we find that the MAPK/ERK pathway regulates eRNA induction, but not H3K27ac accumulation, at rapid enhancers, suggesting that enhancer activation occurs in multiple, mechanistically-separable steps.

H3K27ac is a commonly used mark for enhancer activity (Creyghton et al., 2010; Rada-Iglesias et al., 2011), but we find that H3K27ac accumulates at enhancers even in the presence of MAPK/ERK inhibition, which blocks eRNA (and mRNA) induction. In other contexts, histone acetylation has been shown to accumulate despite blocking eRNA transcription, Pol2 recruitment, or initiation of transcription (Hah et al., 2013; Kaikkonen et al., 2013; Wang et al., 2005). These and other experiments (Zhu et al., 2013) suggest that eRNA transcription may be a better marker for enhancer activation than H3K27ac, more accurately reflecting the extent to which an enhancer is activating transcription at a nearby promoter. Given these findings, our eRNA-seq method may be a particularly useful technique for reliably assaying enhancer activation genome-wide.

### Role of Rapid PRG Protein Products

The protein products of rPRGs may be required for the cell biological changes that occur following a single occurrence of brief neuronal activity. For example, brief single behavioral trials are sufficient both for *Arc* induction in hippocampal region CA3 (Miyashita et al., 2009) and for CA3-dependent spatial learning (Nakazawa et al., 2003), suggesting that *Arc* may be required for this learning. In another example, just 7 min of bicuculline treatment (similar to our 5-min treatment) is sufficient to induce transcription- and MAPK/ERK-dependent long-lasting synchronous bursting of primary neurons (Arnold et al., 2005). We hypothesize that the ARG-dependent cell biological effect of brief activity is due, in large part, to the effect of just a few rPRGs that are not transcription factors (e.g., *Arc*, *Amigo3*). In contrast, physiological responses to prolonged activity, including homeostatic responses like synaptic scaling and firing rate homeostasis (Hengen et al., 2016; Ibata et al., 2008; Turrigiano, 2011), may be

mediated by the protein products of dozens to hundreds of dPRGs and SRGs. Our identification of the MAPK/ERK pathway as structural determinant of the first wave of ARG induction now makes it possible to test the specific function of these first-wave genes in transcription-dependent plasticity. In other words, by defining the contribution of MAPK/ERK to the coupling map, our work should enable manipulation of the coupling map to investigate its functional significance.

## STAR★METHODS

Detailed methods are provided in the online version of this paper and include the following:

- KEY RESOURCES TABLE
- CONTACT FOR REAGENT AND RESOURCE SHARING
- EXPERIMENTAL MODEL AND SUBJECT DETAILS
  - Mouse Primary Neuronal Cultures
  - Rat Primary Neuronal Culture
  - Mice
- METHOD DETAILS
  - RNA Extraction and qPCR
  - NanoString
  - RNA Sequencing
  - Fiber Photometry
  - Western Blotting
  - Immunocytochemistry
  - Chromatin Immunoprecipitation
  - Chromatin Immunoprecipitation Sequencing
  - Luciferase Assays
- QUANTIFICATION AND STATISTICAL ANALYSIS
  - Gene Classification
  - Functional Annotation
  - Nearest-Neighbor Classifier
  - scRNA-Seq Analysis
  - RNA-Seq
  - Analysis of Photometry Signals
  - ChIP-Seq
- DATA AND SOFTWARE AVAILABILITY

## SUPPLEMENTAL INFORMATION

Supplemental Information includes eight figures and eight tables and can be found with this article online at <https://doi.org/10.1016/j.neuron.2018.04.001>.

## ACKNOWLEDGMENTS

We thank: Anastasia Nizhnik (technical assistance); Karen Adelman, Charles Danko, Sandeep R. Datta, Steven Flavell, Harrison Gabel, Michael Greenberg, Elizabeth Hong, Kelly Biotte, Heather Landry, Colin Waters, Emily Low, Ian Hill, and Patricia Rohs (critical reading); Gray laboratory members (helpful discussion throughout the course of the project); Joseph Ling and Matthew Friese (early work on this project). BCH IDDRC, 1U54HD090255 (Fluidigm qPCR) Kevin Gerrish, NIEHS Molecular Genomics Core. Funding: R01 MH101528-01, R01 MH116223-01, Armenian-Harvard, and the Kaneb family (J.M.G. lab); the Intramural Research Program of the National Institute of Environmental Health Sciences, National Institutes of Health Z01 ES100221 (S.M.D. lab); the NSF Graduate Research Fellowship Program DGE1144152, DEG1745303 (K.M.T.); National Institute of Health NRSA (N.R.D.), R00 MH096941 (R.N.S.), Canadian Institute of Health Research (J.-H.C.), NIH New Innovator Award DP2 DK105570, R01 DK109930, McKnight Scholar

Award, Harvard Brain Science Initiative Bipolar Disorder Seed Grant, supported by Kent and Liz Dauten (M.L.A. lab).

## AUTHOR CONTRIBUTIONS

Conceptualization, mouse studies, K.M.T. and J.M.G.; Conceptualization, rat studies, R.N.S. and S.M.D.; Analysis, K.M.T. (lead), N.R.D., R.N.S., C.J.D., M.L.A., and J.M.W.; Investigation and Methodology, K.M.T. (lead), N.R.D., R.N.S., J.-H.C., C.J.D., R.G.P., R.D.J., S.M.C., M.K.W., P.R., C.E.C., and M.L.A.; Visualization, K.M.T.; Writing, K.M.T. (lead) and J.M.G.; Writing – feedback, J.-H.C., N.R.D., S.M.D., R.N.S., R.G.P., C.J.D., and M.L.A.

## DECLARATION OF INTERESTS

The authors declare no competing interests.

Received: May 2, 2017  
 Revised: February 20, 2018  
 Accepted: March 29, 2018  
 Published: April 19, 2018

## REFERENCES

- Ahn, S., Ginty, D.D., and Linden, D.J. (1999). A late phase of cerebellar long-term depression requires activation of CaMKIV and CREB. *Neuron* 23, 559–568.
- Allen, B.L., and Taatjes, D.J. (2015). The Mediator complex: a central integrator of transcription. *Nat. Rev. Mol. Cell Biol.* 16, 155–166.
- Arnold, F.J.L., Hofmann, F., Bengtson, C.P., Wittmann, M., Vanhoutte, P., and Bading, H. (2005). Microelectrode array recordings of cultured hippocampal networks reveal a simple model for transcription and protein synthesis-dependent plasticity. *J. Physiol.* 564, 3–19.
- Atkins, C.M., Selcher, J.C., Petraitis, J.J., Trzaskos, J.M., and Sweatt, J.D. (1998). The MAPK cascade is required for mammalian associative learning. *Nat. Neurosci.* 1, 602–609.
- Blake, J.A., Eppig, J.T., Kadin, J.A., Richardson, J.E., Smith, C.L., and Bult, C.J.; the Mouse Genome Database Group (2017). Mouse Genome Database (MGD)-2017: community knowledge resource for the laboratory mouse. *Nucleic Acids Res.* 45 (D1), D723–D729.
- Chen, Y., Stevens, B., Chang, J., Milbrandt, J., Barres, B.A., and Hell, J.W. (2008). NS21: re-defined and modified supplement B27 for neuronal cultures. *J. Neurosci. Methods* 171, 239–247.
- Chepelev, I., Wei, G., Wangsa, D., Tang, Q., and Zhao, K. (2012). Characterization of genome-wide enhancer-promoter interactions reveals co-expression of interacting genes and modes of higher order chromatin organization. *Cell Res.* 22, 490–503.
- Cho, J.-H., Huang, B.S., and Gray, J.M. (2016). RNA sequencing from neural ensembles activated during fear conditioning in the mouse temporal association cortex. *Sci. Rep.* 6, 31753.
- Creyghton, M.P., Cheng, A.W., Welstead, G.G., Kooistra, T., Carey, B.W., Steine, E.J., Hanna, J., Lodato, M.A., Frampton, G.M., Sharp, P.A., et al. (2010). Histone H3K27ac separates active from poised enhancers and predicts developmental state. *Proc. Natl. Acad. Sci. USA* 107, 21931–21936.
- Dale, R.K., Matzat, L.H., and Lei, E.P. (2014). metaseq: a Python package for integrative genome-wide analysis reveals relationships between chromatin insulators and associated nuclear mRNA. *Nucleic Acids Res.* 42, 9158–9170.
- Davis, S., Vanhoutte, P., Pages, C., Caboche, J., and Laroche, S. (2000). The MAPK/ERK cascade targets both Elk-1 and cAMP response element-binding protein to control long-term potentiation-dependent gene expression in the dentate gyrus in vivo. *J. Neurosci.* 20, 4563–4572.
- De Koninck, P., and Schulman, H. (1998). Sensitivity of CaM kinase II to the frequency of Ca<sup>2+</sup> oscillations. *Science* 279, 227–230.
- Dobin, A., Davis, C.A., Schlesinger, F., Drenkow, J., Zaleski, C., Jha, S., Batut, P., Chaisson, M., and Gingeras, T.R. (2013). STAR: ultrafast universal RNA-seq aligner. *Bioinformatics* 29, 15–21.

- Dolmetsch, R.E., Lewis, R.S., Goodnow, C.C., and Healy, J.I. (1997). Differential activation of transcription factors induced by Ca<sup>2+</sup> response amplitude and duration. *Nature* 386, 855–858.
- Dolmetsch, R.E., Xu, K., and Lewis, R.S. (1998). Calcium oscillations increase the efficiency and specificity of gene expression. *Nature* 392, 933–936.
- Dolmetsch, R.E., Pajvani, U., Fife, K., Spotts, J.M., and Greenberg, M.E. (2001). Signaling to the nucleus by an L-type calcium channel-calmodulin complex through the MAP kinase pathway. *Science* 294, 333–339.
- Douglas, R.M., Dragunow, M., and Robertson, H.A. (1988). High-frequency discharge of dentate granule cells, but not long-term potentiation, induces c-fos protein. *Brain Res.* 464, 259–262.
- Dudek, S.M., and Fields, R.D. (2001). Mitogen-activated protein kinase/extracellular signal-regulated kinase activation in somatodendritic compartments: roles of action potentials, frequency, and mode of calcium entry. *J. Neurosci.* 21, RC122.
- ENCODE Project Consortium (2012). An integrated encyclopedia of DNA elements in the human genome. *Nature* 489, 57–74.
- Eriksson, M., Taskinen, M., and Leppä, S. (2007). Mitogen activated protein kinase-dependent activation of c-Jun and c-Fos is required for neuronal differentiation but not for growth and stress response in PC12 cells. *J. Cell. Physiol.* 210, 538–548.
- Escoubet-Lozach, L., Benner, C., Kaikkonen, M.U., Lozach, J., Heinz, S., Spann, N.J., Crotti, A., Stender, J., Ghisletti, S., Reichart, D., et al. (2011). Mechanisms establishing TLR4-responsive activation states of inflammatory response genes. *PLoS Genet.* 7, e1002401.
- Eshete, F., and Fields, R.D. (2001). Spike frequency decoding and autonomous activation of Ca<sup>2+</sup>-calmodulin-dependent protein kinase II in dorsal root ganglion neurons. *J. Neurosci.* 21, 6694–6705.
- Evans, M.D., Sammons, R.P., Lebron, S., Dumitrescu, A.S., Watkins, T.B.K., Uebele, V.N., Renger, J.J., and Grubb, M.S. (2013). Calcineurin signaling mediates activity-dependent relocation of the axon initial segment. *J. Neurosci.* 33, 6950–6963.
- Favata, M.F., Horiuchi, K.Y., Manos, E.J., Daulerio, A.J., Stradley, D.A., Feeser, W.S., Van Dyk, D.E., Pitts, W.J., Earl, R.A., Hobbs, F., et al. (1998). Identification of a novel inhibitor of mitogen-activated protein kinase kinase. *J. Biol. Chem.* 273, 18623–18632.
- Fields, R.D., Eshete, F., Stevens, B., and Itoh, K. (1997). Action potential-dependent regulation of gene expression: temporal specificity in Ca<sup>2+</sup>, cAMP-responsive element binding proteins, and mitogen-activated protein kinase signaling. *J. Neurosci.* 17, 7252–7266.
- Flavell, S.W., and Greenberg, M.E. (2008). Signaling mechanisms linking neuronal activity to gene expression and plasticity of the nervous system. *Annu. Rev. Neurosci.* 31, 563–590.
- Fowler, T., Sen, R., and Roy, A.L. (2011). Regulation of primary response genes. *Mol. Cell* 44, 348–360.
- Fujii, H., Inoue, M., Okuno, H., Sano, Y., Takemoto-Kimura, S., Kitamura, K., Kano, M., and Bito, H. (2013). Nonlinear decoding and asymmetric representation of neuronal input information by CaMKIIα and calcineurin. *Cell Rep.* 3, 978–987.
- Gaidatzis, D., Burger, L., Florescu, M., and Stadler, M.B. (2015). Analysis of intronic and exonic reads in RNA-seq data characterizes transcriptional and post-transcriptional regulation. *Nat. Biotechnol.* 33, 722–729.
- Gilchrist, D.A., Dos Santos, G., Fargo, D.C., Xie, B., Gao, Y., Li, L., and Adelman, K. (2010). Pausing of RNA polymerase II disrupts DNA-specified nucleosome organization to enable precise gene regulation. *Cell* 143, 540–551.
- Gotoh, Y., Nishida, E., Yamashita, T., Hoshi, M., Kawakami, M., and Sakai, H. (1990). Microtubule-associated-protein (MAP) kinase activated by nerve growth factor and epidermal growth factor in PC12 cells. Identity with the mitogen-activated MAP kinase of fibroblastic cells. *Eur. J. Biochem.* 193, 661–669.
- Gray, J.M., Harmin, D.A., Boswell, S.A., Cloonan, N., Mullen, T.E., Ling, J.J., Miller, N., Kuersten, S., Ma, Y.C., McCarroll, S.A., et al. (2014). SnapShot-Seq: a method for extracting genome-wide, *in vivo* mRNA dynamics from a single total RNA sample. *PLoS ONE* 9, e89673.
- Greenberg, M.E., Ziff, E.B., and Greene, L.A. (1986). Stimulation of neuronal acetylcholine receptors induces rapid gene transcription. *Science* 234, 80–83.
- Hah, N., Murakami, S., Nagari, A., Danko, C.G., and Kraus, W.L. (2013). Enhancer transcripts mark active estrogen receptor binding sites. *Genome Res.* 23, 1210–1223.
- Hardingham, G.E., Arnold, F.J.L., and Bading, H. (2001). A calcium microdomain near NMDA receptors: on switch for ERK-dependent synapse-to-nucleus communication. *Nat. Neurosci.* 4, 565–566.
- Hargreaves, D.C., Hornig, T., and Medzhitov, R. (2009). Control of inducible gene expression by signal-dependent transcriptional elongation. *Cell* 138, 129–145.
- Hengen, K.B., Torrado Pacheco, A., McGregor, J.N., Van Hooser, S.D., and Turrigiano, G.G. (2016). Neuronal firing rate homeostasis is inhibited by sleep and promoted by wake. *Cell* 165, 180–191.
- Herschman, H.R. (1991). Primary response genes induced by growth factors and tumor promoters. *Annu. Rev. Biochem.* 60, 281–319.
- Hrvatin, S., Hochbaum, D.R., Nagy, M.A., Cicconet, M., Robertson, K., Cheadle, L., Zilionis, R., Ratner, A., Borges-Moroy, R., Klein, A.M., et al. (2018). Single-cell analysis of experience-dependent transcriptomic states in the mouse visual cortex. *Nat. Neurosci.* 21, 120–129.
- Hu, P., Fabyanic, E., Kwon, D.Y., Tang, S., Zhou, Z., and Wu, H. (2017). Dissecting cell-type composition and activity-dependent transcriptional state in mammalian brains by massively parallel single-nucleus RNA-seq. *Mol. Cell* 68, 1006–1015.e7.
- Hunter, J.D. (2007). Matplotlib: a 2D graphics environment. *Comput. Sci. Eng.* 9, 99–104.
- Ibata, K., Sun, Q., and Turrigiano, G.G. (2008). Rapid synaptic scaling induced by changes in postsynaptic firing. *Neuron* 57, 819–826.
- Joo, J.-Y., Schaukowitch, K., Farbiak, L., Kilaru, G., and Kim, T.-K. (2016). Stimulus-specific combinatorial functionality of neuronal c-fos enhancers. *Nat. Neurosci.* 19, 75–83.
- Jun, J.J., Steinmetz, N.A., Siegle, J.H., Denman, D.J., Bauza, M., Barbarits, B., Lee, A.K., Anastassiou, C.A., Andrei, A., Aydin, C., et al. (2017). Fully integrated silicon probes for high-density recording of neural activity. *Nature* 551, 232–236.
- Kaikkonen, M.U., Spann, N.J., Heinz, S., Romanoski, C.E., Allison, K.A., Stender, J.D., Chun, H.B., Tough, D.F., Prinjha, R.K., Benner, C., and Glass, C.K. (2013). Remodeling of the enhancer landscape during macrophage activation is coupled to enhancer transcription. *Mol. Cell* 51, 310–325.
- Kim, T.-K., Hemberg, M., Gray, J.M., Costa, A.M., Bear, D.M., Wu, J., Harmin, D.A., Laptevich, M., Barbara-Haley, K., Kuersten, S., et al. (2010). Widespread transcription at neuronal activity-regulated enhancers. *Nature* 465, 182–187.
- Kingsbury, T.J., Bambrick, L.L., Roby, C.D., and Krueger, B.K. (2007). Calcineurin activity is required for depolarization-induced, CREB-dependent gene transcription in cortical neurons. *J. Neurochem.* 103, 761–770.
- Kuhn, R.M., Haussler, D., and Kent, W.J. (2013). The UCSC genome browser and associated tools. *Brief. Bioinform.* 14, 144–161.
- Lacar, B., Linker, S.B., Jaeger, B.N., Krishnaswami, S., Barron, J., Kelder, M., Parylak, S., Paquola, A., Venepally, P., Novotny, M., et al. (2016). Nuclear RNA-seq of single neurons reveals molecular signatures of activation. *Nat. Commun.* 7, 11022.
- Langmead, B., and Salzberg, S.L. (2012). Fast gapped-read alignment with Bowtie 2. *Nat. Methods* 9, 357–359.
- Lee, P.R., Cohen, J.E., Iacobas, D.A., Iacobas, S., and Fields, R.D. (2017). Gene networks activated by specific patterns of action potentials in dorsal root ganglia neurons. *Sci. Rep.* 7, 43765.
- Li, H., Handsaker, B., Wysoker, A., Fennell, T., Ruan, J., Homer, N., Marth, G., Abecasis, G., and Durbin, R. (2009). The Sequence Alignment/Map format and SAMtools. *Bioinformatics* 25, 2078–2079.

- Ma, H., Groth, R.D., Wheeler, D.G., Barrett, C.F., and Tsien, R.W. (2011). Excitation-transcription coupling in sympathetic neurons and the molecular mechanism of its initiation. *Neurosci. Res.* 70, 2–8.
- Marais, R., Wynne, J., and Treisman, R. (1993). The SRF accessory protein Elk-1 contains a growth factor-regulated transcriptional activation domain. *Cell* 73, 381–393.
- Marshall, C.J. (1995). Specificity of receptor tyrosine kinase signaling: transient versus sustained extracellular signal-regulated kinase activation. *Cell* 80, 179–185.
- Mi, H., Huang, X., Muruganujan, A., Tang, H., Mills, C., Kang, D., and Thomas, P.D. (2017). PANTHER version 11: expanded annotation data from Gene Ontology and Reactome pathways, and data analysis tool enhancements. *Nucleic Acids Res.* 45 (D1), D183–D189.
- Miyashita, T., Kubik, S., Haghghi, N., Steward, O., and Guzowski, J.F. (2009). Rapid activation of plasticity-associated gene transcription in hippocampal neurons provides a mechanism for encoding of one-trial experience. *J. Neurosci.* 29, 898–906.
- Mohammed, A.I., Gritton, H.J., Tseng, H.A., Bucklin, M.E., Yao, Z., and Han, X. (2016). An integrative approach for analyzing hundreds of neurons in task performing mice using wide-field calcium imaging. *Sci. Rep.* 6, 20986.
- Murphy, T.H., Blatter, L.A., Bhat, R.V., Fiore, R.S., Wier, W.G., and Baraban, J.M. (1994). Differential regulation of calcium/calmodulin-dependent protein kinase II and p42 MAP kinase activity by synaptic transmission. *J. Neurosci.* 14, 1320–1331.
- Nakazawa, K., Sun, L.D., Quirk, M.C., Rondi-Reig, L., Wilson, M.A., and Tonegawa, S. (2003). Hippocampal CA3 NMDA receptors are crucial for memory acquisition of one-time experience. *Neuron* 38, 305–315.
- Nguyen, P.V., Abel, T., and Kandel, E.R. (1994). Requirement of a critical period of transcription for induction of a late phase of LTP. *Science* 265, 1104–1107.
- Nguyen, T.A., Jones, R.D., Snively, A.R., Pfennig, A.R., Kirchner, R., Hemberg, M., and Gray, J.M. (2016). High-throughput functional comparison of promoter and enhancer activities. *Genome Res.* 26, 1023–1033.
- Quinlan, A.R., and Hall, I.M. (2010). BEDTools: a flexible suite of utilities for comparing genomic features. *Bioinformatics* 26, 841–842.
- Rada-Iglesias, A., Bajpai, R., Swigut, T., Brugmann, S.A., Flynn, R.A., and Wysocka, J. (2011). A unique chromatin signature uncovers early developmental enhancers in humans. *Nature* 470, 279–283.
- Ramanan, N., Shen, Y., Sarsfield, S., Lemberger, T., Schütz, G., Linden, D.J., and Ginty, D.D. (2005). SRF mediates activity-induced gene expression and synaptic plasticity but not neuronal viability. *Nat. Neurosci.* 8, 759–767.
- Ramirez-Carrozzi, V.R., Nazarian, A.A., Li, C.C., Gore, S.L., Sridharan, R., Imbalzano, A.N., and Smale, S.T. (2006). Selective and antagonistic functions of SWI/SNF and Mi-2beta nucleosome remodeling complexes during an inflammatory response. *Genes Dev.* 20, 282–296.
- Ramirez-Carrozzi, V.R., Braas, D., Bhatt, D.M., Cheng, C.S., Hong, C., Doty, K.R., Black, J.C., Hoffmann, A., Carey, M., and Smale, S.T. (2009). A unifying model for the selective regulation of inducible transcription by CpG islands and nucleosome remodeling. *Cell* 138, 114–128.
- Robinson, M.D., McCarthy, D.J., and Smyth, G.K. (2010). edgeR: a Bioconductor package for differential expression analysis of digital gene expression data. *Bioinformatics* 26, 139–140.
- Saha, R.N., Wissink, E.M., Bailey, E.R., Zhao, M., Fargo, D.C., Hwang, J.-Y., Daigle, K.R., Fenn, J.D., Adelman, K., and Dudek, S.M. (2011). Rapid activity-induced transcription of Arc and other IEGs relies on poised RNA polymerase II. *Nat. Neurosci.* 14, 848–856.
- Santos, S.D.M., Verveer, P.J., and Bastiaens, P.I.H. (2007). Growth factor-induced MAPK network topology shapes Erk response determining PC-12 cell fate. *Nat. Cell Biol.* 9, 324–330.
- Sgambato, V., Vanhoutte, P., Pagès, C., Rogard, M., Hipskind, R., Besson, M.J., and Caboche, J. (1998). In vivo expression and regulation of Elk-1, a target of the extracellular-regulated kinase signaling pathway, in the adult rat brain. *J. Neurosci.* 18, 214–226.
- Shao, Z., Zhang, Y., Yuan, G.-C., Orkin, S.H., and Waxman, D.J. (2012). MANorm: a robust model for quantitative comparison of ChIP-seq data sets. *Genome Biol.* 13, R16.
- Sheng, H.Z., Fields, R.D., and Nelson, P.G. (1993). Specific regulation of immediate early genes by patterned neuronal activity. *J. Neurosci. Res.* 35, 459–467.
- Shepherd, J.D., and Bear, M.F. (2011). New views of Arc, a master regulator of synaptic plasticity. *Nat. Neurosci.* 14, 279–284.
- Spiegel, I., Mardinly, A.R., Gabel, H.W., Bazinet, J.E., Couch, C.H., Tzeng, C.P., Harmin, D.A., and Greenberg, M.E. (2014). Npas4 regulates excitatory-inhibitory balance within neural circuits through cell-type-specific gene programs. *Cell* 157, 1216–1229.
- Szutorisz, H., Dillon, N., and Tora, L. (2005). The role of enhancers as centres for general transcription factor recruitment. *Trends Biochem. Sci.* 30, 593–599.
- Tasic, B., Menon, V., Nguyen, T.N., Kim, T.K., Jarsky, T., Yao, Z., Levi, B., Gray, L.T., Sorensen, S.A., Dolbeare, T., et al. (2016). Adult mouse cortical cell taxonomy revealed by single cell transcriptomics. *Nat. Neurosci.* 19, 335–346.
- Telesio, F., Ma, Q., Perez, P.M., Notani, D., Oh, S., Li, W., Comoletti, D., Ohgi, K.A., Taylor, H., and Rosenfeld, M.G. (2015). LRP8-Reelin-regulated neuronal enhancer signature underlying learning and memory formation. *Neuron* 86, 696–710.
- Thomas, G.M., and Huganir, R.L. (2004). MAPK cascade signalling and synaptic plasticity. *Nat. Rev. Neurosci.* 5, 173–183.
- Toettcher, J.E., Weiner, O.D., and Lim, W.A. (2013). Using optogenetics to interrogate the dynamic control of signal transmission by the Ras/Erk module. *Cell* 155, 1422–1434.
- Trapnell, C., Cacchiarelli, D., Grimsby, J., Pokharel, P., Li, S., Morse, M., Lennon, N.J., Livak, K.J., Mikkelsen, T.S., and Rinn, J.L. (2014). The dynamics and regulators of cell fate decisions are revealed by pseudotemporal ordering of single cells. *Nat. Biotechnol.* 32, 381–386.
- Treisman, R. (1996). Regulation of transcription by MAP kinase cascades. *Curr. Opin. Cell Biol.* 8, 205–215.
- Tullai, J.W., Schaffer, M.E., Mullenbrock, S., Sholder, G., Kasif, S., and Cooper, G.M. (2007). Immediate-early and delayed primary response genes are distinct in function and genomic architecture. *J. Biol. Chem.* 282, 23981–23995.
- Turrigiano, G. (2011). Too many cooks? Intrinsic and synaptic homeostatic mechanisms in cortical circuit refinement. *Annu. Rev. Neurosci.* 34, 89–103.
- Van Der Walt, S., Colbert, S.C., and Varoquaux, G. (2011). The NumPy array: a structure for efficient numerical computation. *Comput. Sci. Eng.* 13, 22–30.
- Wang, G., Balamotis, M.A., Stevens, J.L., Yamaguchi, Y., Handa, H., and Berk, A.J. (2005). Mediator requirement for both recruitment and postrecruitment steps in transcription initiation. *Mol. Cell* 17, 683–694.
- Worley, P.F., Bhat, R.V., Baraban, J.M., Erickson, C.A., McNaughton, B.L., and Barnes, C.A. (1993). Thresholds for synaptic activation of transcription factors in hippocampus: correlation with long-term enhancement. *J. Neurosci.* 13, 4776–4786.
- Wu, G.Y., Deisseroth, K., and Tsien, R.W. (2001a). Spaced stimuli stabilize MAPK pathway activation and its effects on dendritic morphology. *Nat. Neurosci.* 4, 151–158.
- Wu, G.Y., Deisseroth, K., and Tsien, R.W. (2001b). Activity-dependent CREB phosphorylation: convergence of a fast, sensitive calmodulin kinase pathway and a slow, less sensitive mitogen-activated protein kinase pathway. *Proc. Natl. Acad. Sci. USA* 98, 2808–2813.
- Wu, Y.E., Pan, L., Zuo, Y., Li, X., and Hong, W. (2017). Detecting activated cell populations using single-cell RNA-seq. *Neuron* 96, 313–329.e6.

- Xia, Z., Dudek, H., Miranti, C.K., and Greenberg, M.E. (1996). Calcium influx via the NMDA receptor induces immediate early gene transcription by a MAP kinase/ERK-dependent mechanism. *J. Neurosci.* **16**, 5425–5436.
- Ye, C., Speed, T.P., and Salim, A. (2017). DECENT: differential expression with capture efficiency adjustment for single-cell RNA-seq data. *bioRxiv*, doi: 10.1101/225177.
- Yu, Y., Oberlaender, K., Bengtson, C.P., and Bading, H. (2017). One nuclear calcium transient induced by a single burst of action potentials represents the minimum signal strength in activity-dependent transcription in hippocampal neurons. *Cell Calcium* **65**, 14–21.
- Zhai, S., Ark, E.D., Parra-Bueno, P., and Yasuda, R. (2013). Long-distance integration of nuclear ERK signaling triggered by activation of a few dendritic spines. *Science* **342**, 1107–1111.
- Zheng, F., Luo, Y., and Wang, H. (2009). Regulation of brain-derived neurotrophic factor-mediated transcription of immediate early gene Arc by intracellular calcium and calmodulin. *J. Neurosci. Res.* **87**, 380–392.
- Zhu, Y., Sun, L., Chen, Z., Whitaker, J.W., Wang, T., and Wang, W. (2013). Predicting enhancer transcription and activity from chromatin modifications. *Nucleic Acids Res.* **41**, 10032–10043.

**STAR★METHODS****KEY RESOURCES TABLE**

REAGENT or RESOURCE	SOURCE	IDENTIFIER
<b>Antibodies</b>		
Rabbit anti-phospho-ERK1/2	Cell Signaling Technology	Cat# 4370; RRID: AB_2315112
Mouse anti-GAPDH	Thermo Fisher Scientific	Cat# MA5-15738; RRID: AB_2537652
Rabbit anti-ARC	Synaptic Systems	Cat# 156-003; RRID: AB_2151848
Mouse anti-phospho-Elk-1 (Clone B4)	Santa Cruz	Cat# sc-8406X; RRID: AB_627509
Rabbit anti-GAPDH (D16H11)	Cell Signaling Technology	Cat# 2118S; RRID: AB_10622025
Mouse anti-H4	Cell Signaling Technology	Cat# 2935; RRID: AB_1147658
Mouse anti-Beta-actin	Millipore	Cat# AM4302; RRID: AB_2536382
Rabbit anti-phospho-CaMKIV	Santa Cruz	Cat# sc28443-R; RRID: AB_2068399
Rabbit anti-H3K27ac	Abcam	Cat# ab4729; RRID: AB_2118291
Mouse anti-RNA polymerase II CTD repeat YSPTSPS [8WG16]	Abcam	Cat# ab817; RRID:AB_306327
Mouse anti-Beta-actin (8H10D10)	Cell Signaling Technology	Cat#3700; RRID: AB_2242334
IRDye 680RD Goat anti-Rabbit IgG (H + L)	LI-COR	Cat# P/N 925-68071; RRID: AB_2721181
IRDye 680RD Goat anti-Mouse IgG (H + L)	LI-COR	Cat# P/N 925-68070; RRID: AB_2651128
Goat anti-Rabbit IgG (H+L) Secondary Antibody, Alexa Fluor 594	Thermo Fisher Scientific	Cat# R37117; RRID: AB_2556545
Goat anti-Mouse IgG (H+L) Cross-Adsorbed Secondary Antibody, Alexa Fluor 680	Thermo Fisher Scientific	Cat# A-21057 RRID: AB_2535723
<b>Bacterial and Virus Strains</b>		
AAV1.Syn.GCaMP6s.WPRE.SV40	Penn Vector Core	Cat# AV-PV2824
pTAN02 luciferase assay plasmid	<a href="#">Nguyen et al., 2016</a>	PMCID: PMC4971761
<b>Chemicals, Peptides, and Recombinant Proteins</b>		
Poly-ornithine	Sigma	Cat# P3655-100MG
Papain	Worthington	Cat# (L)(S)003126
B27 (Gray lab)	Thermo Fisher Scientific	Cat# 17504001
B27 (Saha lab)	Thermo Fisher Scientific	Cat# A3582801
DL-AP5 Sodium Salt	Tocris	Cat# 3693
NBQX	Tocris	Cat# 0373
U0126	Tocris	Cat# 1144
11e	Tocris	Cat# 4465
STO-609	Tocris	Cat# 1551
Cycloheximide	Cell Signaling Technology	Cat# 2112
PD183452	Tocris	Cat# 4237
Triptolide	Tocris	Cat# 3253
Bicuculline	Sigma	Cat# 14340
Aminopyridine	Acros Organics	Cat# 104570250
TTX	MedChemExpress	Cat# HY-12526
SL327	Tocris	Cat# 1969
Actinomycin D	Sigma	Cat# A1410-5MG
Protease inhibitor cocktail	Roche	Cat# 05056489001
PhosStop phosphatase inhibitor	Roche	Cat# 04906837001
<b>Critical Commercial Assays</b>		
Megascript SP6 <i>In Vitro</i> Transcription kit	Thermo Fisher Scientific	Cat# AM1330
NuGen Ultralow V2 1-96 library prep kit	NuGen	Cat# 0347

(Continued on next page)

***Continued***

REAGENT or RESOURCE	SOURCE	IDENTIFIER
Dual-Luciferase Reporter Assay System	Promega	Cat# E1910
High Capacity cDNA RT Kit	Applied BioSystems	Cat# 4368814
RNase-Free DNase Set	QIAGEN	Cat# 79254
ERCC RNA Spike-In Mix	Ambion	Cat# 4456740
TruSeq Stranded Total RNA Library Prep Human/Mouse/Rat (96 Samples)	Illumina	Cat# RS-122-2303
<b>Deposited Data</b>		
RNA-seq, ChIP-seq (SRF, CREB, Pol2)	Kim et al., 2010	GEO: GSE21161
ChIP-seq (MEF2, MEF2C, H3K4me2, H4K16ac, NCoR, MED23, MED1, H3K27ac/H4K16ac in hippocampus)	Telese et al., 2015	GEO: GSE66710
DNase I HS from 8w cerebrum	ENCODE Project Consortium, Stamatoyannopoulos - UW	GEO: GSM1014168, UCSC: wgEncodeEM001718
scRNA-seq data	Hrvatin et al., 2018	GEO: GSE102827
RNA-seq and ChIP-seq	This paper	GEO: GSE111899
<b>Experimental Models: Organisms/Strains</b>		
C57BL/6NCrl	Charles River	RRID: IMSR_CRL:27
Sprague Dawley strain rat	Charles River	RRID: SCR_003792
Crl:CD1(ICR) mouse	Charles River	RRID: IMSR_CRL:22
<b>Oligonucleotides</b>		
RNA-capture-seq probes (DNA oligonucleotides) (ARG-seq)	Custom Array; this paper	<a href="#">Table S1</a>
RNA-capture-seq probes (DNA oligonucleotides) (eRNA-seq)	Twist Biosciences; this paper	<a href="#">Table S1</a>
DNA primers (qPCR)	This paper	<a href="#">Table S6</a>
Capture-seq blocking primer: p5-AATGATACGG CGACCACCGAGATCTACAC	This paper	N/A
Capture-seq blocking primer: ACACTCTTCCCT ACACGACGCTCTCCGATC/3InvdT/ p7- 164 CAAGCAGAAGACGGCATACGAGAT	This paper	N/A
Capture-seq blocking primer: GTGACTGGAG TTCAGACGTGT 165 GCTCTTCGATC/3InvdT/	This paper	N/A
Capture-seq amplification primer: p5-AATGA TACGGCGACCACCGAGA	This paper	N/A
Capture-seq amplification primer: p7-CAAGC AGAAGACGGCATACGAG	This paper	N/A
Fos e5 cloning F: ATACGGTACCCGAGACT ACGTCA	This paper	N/A
Fos e5 cloning R: ATGTCTCGAGATTAAAAAA GGCCC	This paper	N/A
Taq-man probes used with Fluidigm high-throughput qPCR	Invitrogen; this paper	<a href="#">Table S3</a>
NanoString probes	This paper	<a href="#">Table S4</a>
<b>Software and Algorithms</b>		
STAR aligner	Dobin et al., 2013	<a href="https://github.com/alexdobin/STAR/">https://github.com/alexdobin/STAR/</a> ; RRID: SCR_015899
SAMtools	Li et al., 2009	<a href="http://samtools.sourceforge.net/">http://samtools.sourceforge.net/</a> ; RRID: SCR_002105
BEDtools	Quinlan and Hall, 2010	<a href="http://bedtools.readthedocs.io/en/latest/">http://bedtools.readthedocs.io/en/latest/</a> ; RRID: SCR_015899
UCSC-tools	Kuhn et al., 2013	<a href="http://hgdownload.soe.ucsc.edu/admin/exe/">http://hgdownload.soe.ucsc.edu/admin/exe/</a>

*(Continued on next page)*

***Continued***

REAGENT or RESOURCE	SOURCE	IDENTIFIER
EdgeR	Robinson et al., 2010	<a href="http://bioconductor.org/packages/release/bioc/html/edgeR.html">http://bioconductor.org/packages/release/bioc/html/edgeR.html</a> ; RRID: SCR_012802
Bowtie2	Langmead and Salzberg, 2012	<a href="http://bowtie-bio.sourceforge.net/bowtie2/index.shtml">http://bowtie-bio.sourceforge.net/bowtie2/index.shtml</a>
Metaseq	Dale et al., 2014	<a href="https://pythonhosted.org/metaseq/">https://pythonhosted.org/metaseq/</a>
NumPy	Van Der Walt et al., 2011	<a href="http://www.numpy.org/">http://www.numpy.org/</a> ; RRID: SCR_008633
Matplotlib	Hunter, 2007	<a href="https://matplotlib.org/downloads.html">https://matplotlib.org/downloads.html</a> ; RRID: SCR_008624
PANTHER v.13.1	Mi et al., 2017	<a href="http://www.pantherdb.org/downloads/">http://www.pantherdb.org/downloads/</a> ; RRID: SCR_004869
MATLAB	MathWorks	<a href="https://www.mathworks.com/products/matlab.html">https://www.mathworks.com/products/matlab.html</a> ; RRID: SCR_001622
Other		
MyOne Streptavidin T1 Dynabeads	Invitrogen	Cat# 65601
Herculase II Fusion polymerase	Agilent	Cat# 600675
Protein A Dynabeads	Thermo Fisher Scientific	Cat# 10001D; Cat# 10002D
Protein G Dynabeads	Thermo Fisher Scientific	Cat# 10003D; Cat# 10004D
RNase A	Ambion, Life Technology	Cat# AM2271
Proteinase K	New England Biolabs	Cat# P8107S
Drosophila spike-in chromatin	Active Motif	Cat #61686; Cat# 53083
SsoFast EvaGreen Supermix (qPCR)	Bio-Rad	Cat# 172-5204
TRIzol	Invitrogen	Cat# 15596018
Human Cot-1 DNA	Thermo Fisher Scientific	Cat# 18440-016
Salmon Sperm DNA Solution	Thermo Fisher Scientific	Cat# 15632-011
UltraPure 20X SSPE	Life Technologies	Cat# 15591-043
M-MLV Reverse Transcriptase	Promega	Cat# M1701
Random Primers	Promega	Cat# C1181
Oligo-dt Primers	Promega	Cat# C1101
RNase inhibitor	Thermo Fisher Scientific	Cat# EO0382
iTaq Universal SYBR Green Supermix	BioRad	Cat# 1725124
PerfeCTa SYBR Green FastMix	QuantaBio	Cat# 95071-012
Neurobasal Medium	Thermo Fisher Scientific (Gray lab); Thermo Fisher Scientific (Saha lab)	Cat# 12348-017; Cat# 21103049
GlutaMAX Supplement	Thermo Fisher Scientific	Cat# 35050-061
Penicillin-streptomycin	Thermo Fisher Scientific	Cat# 15140122
NuPAGE 4%–12% Bis-Tris Protein Gels, 1.5 mm, 15-well	Life Technology	Cat# NP0336BOX
RNeasy Mini Kit	QIAGEN	Cat# 74106
RNase-free DNase	QIAGEN	Cat# 79254
One-Step RT-PCR kit	QIAGEN	Cat# 210210
QIAGEN MinElute Reaction CleanUp Kit	QIAGEN	Cat# 28204
QIAGEN MinElute PCR CleanUp Kit	QIAGEN	Cat# 28004

**CONTACT FOR REAGENT AND RESOURCE SHARING**

Further information and requests for resources and reagents should be directed to and will be fulfilled by the Lead Contact, Jesse Gray ([gray@genetics.med.harvard.edu](mailto:gray@genetics.med.harvard.edu)).

## EXPERIMENTAL MODEL AND SUBJECT DETAILS

### Mouse Primary Neuronal Cultures

#### Culture

Cortical neurons were dissected from embryonic day 16 (E16) CD1 embryos of mixed sex. They were dissociated with papain (Worthington, (L)(S)003126) and plated on plates coated for at least 1 hr with poly-ornithine (30mg/mL, Sigma) in water and then washed three times with water. They were maintained at 37°C at 5% CO<sub>2</sub> in neurobasal media (ThermoFisher) supplemented with B27 (ThermoFisher), Glutamax (ThermoFisher), and penicillin/streptomycin (ThermoFisher).

#### Stimulation

At 6 or 7 days *in vitro* (DIV), neurons were silenced with APV (100μM, Tocris) and NBQX (10μM, Tocris) to block NMDA and AMPA receptors. 14–16 hr later neurons were stimulated with a final concentration of 55mM potassium chloride (KCl) using KCl depolarization solution (170mM KCl, 10mM HEPES pH 7.4, 1mM MgCl<sub>2</sub>, 2mM CaCl<sub>2</sub>). For sustained stimulation, KCl was left on neurons for up to 6 hr, whereas for brief stimulation, it was added for 1 min and then removed and replaced with conditioned neurobasal supplemented with APV and NBQX until RNA collection. While sustained KCl-mediated depolarization elevates intracellular calcium for a minimum of 20 min and likely indefinitely (Dolmetsch et al., 2001; Evans et al., 2013), brief KCl-mediated depolarization elevates intracellular calcium only during the period of elevated KCl (Kingsbury et al., 2007). 10 μM U0126 (Tocris), 625nM 11e (Tocris), 3 μM STO-609 (Tocris), 30 μM cycloheximide (Cell Signaling) or DMSO (equal volume) were added 30 min before stimulation and left on the neurons throughout the experiment. 10 μg/mL ActinomycinD (Sigma) was added 15 min before stimulation. 10 μM triptolide (Tocris) was added 5 min before stimulation.

### Rat Primary Neuronal Culture

#### Culture

Cultures of cortical neurons were prepared from embryonic day 18 Sprague Dawley rats of mixed sex (NIEHS Animal Study Proposal #01-21). Dissociated cortical neurons were plated in Neurobasal medium (Invitrogen) supplemented with 25mM glutamate (Sigma-Aldrich) and 0.5 mM L-glutamine (Sigma-Aldrich) and either B27 (Invitrogen) or NS21 and maintained in a similar medium without the glutamate. NS21 was prepared in the laboratory (Chen et al., 2008). Cultures were grown at 37°C with 5% CO<sub>2</sub>.

#### Stimulation

Neurons were used routinely between 10–14DIV. To induce synaptic stimulation, we triggered neuronal activity by co-treating neurons with 50μM Bicuculline (Sigma-Aldrich) and 75μM 4-Aminopyridine (Acros Organics) (or a DMSO control). To induce brief activity, activity was ceased at the desired time point (5 min or 10 s) using 2μM TTX. Neurons were collected at various time points. 2μM PD184352 (Tocris) was added with bicuculline. 10μM U0126 was added 30 min before treatment with bicuculline.

### Mice

#### Animal Care

All animal care and experimental procedures were approved by the Institutional Animal Care and Use Committees at each institution. Animals were housed with standard mouse chow and water provided *ad libitum*. Male C57BL/6J adult male mice (6–14 weeks old) were used for *in vivo* experiments in this study.

#### Visual Stimulation

For the flashing-light visual stimulation used in experiments with qPCR-based gene expression analysis and photometry, adult mice were first housed in the dark for three days (for gene expression) or 12 hr (for photometry). Mice were housed with 3 mice per cage (for gene expression) or single-housed (for photometry). Bright lights (two GE White 18" Fluorescent Light Fixtures, part # UCF18P and F15T8, 15W/60Hz) placed on either side of the mouse home cage were then used for the stimulation. Sustained stimulation was achieved by repeated 60 s of illumination followed by 20 s of darkness for up to 4 hr. For intermediate (7 min) and brief (1 min) stimulation, the cage was illuminated using the same program, but stopping after 7 or 1 min, respectively, followed by waiting for up to 4 hr in the dark before tissue collection. This illumination schedule was achieved using a Raspberry Pi B (Model #756-8308) and relay (Adafruit Controllable Four Outlet Power Relay Module ID#: 2935). For gene expression experiments, at several time points following the start of stimulation, mice were sacrificed using carbon dioxide, eyes were enucleated, both visual cortices were separately dissected and homogenized in Trizol (Invitrogen) for subsequent qPCR.

For *in vivo* experiments testing the effects of MEK inhibition, mice were singly dark-housed for 3 days. The stimulus consisted of turning on the room lights either continuously or briefly (for 1 min). On the day of the experiment, mice were intraperitoneally injected with 100mg/kg of SL327 (Tocris), a blood-brain-barrier-crossing analog of U0126 (Atkins et al., 1998), in corn oil or with a corn oil vehicle. Injections started 30 min before visual stimulus and continued once per hour for the duration of the experiment to maintain the effects of the drug. SL327 was solubilized first in 100% ethanol. Then this ethanol mixture was added to corn oil and vortexed for 30 min. The ethanol was then removed from the mixture using a speed vac. The vehicle was prepared in the same way using just ethanol and corn oil without any drug. Mice were sacrificed using carbon dioxide before the stimulus or either 30 min or 2.5 hr after turning on the lights. After enucleating the eyes, their visual cortices were immediately dissected. One hemisphere from each mouse was homogenized in Trizol (Invitrogen) for subsequent ARG-seq, and the other was homogenized in cold lysis buffer (see [Western Blotting](#)) for western blotting to confirm ERK activation.

## METHOD DETAILS

### RNA Extraction and qPCR

#### Mouse Neurons/Cortex

Samples were collected in Trizol (Invitrogen), and total RNA was extracted using the RNeasy mini kit (QIAGEN) with in-column DNase treatment (QIAGEN) according to the instructions of the manufacturer. The RNA was then either used for RNA-seq (see below) or converted to cDNA using the High Capacity cDNA Reverse Transcription kit (Applied Biosystems). For standard qPCR experiments, we used SsoFast Evagreen supermix (BioRad) with primers in [Table S6](#). For high-throughput qPCR, we used Taq-man qPCR probes (designed by Invitrogen) using the Fluidigm microfluidics system (see [Table S3](#)). High-throuput qPCR was performed by the BCH IDDRC, 1U54HD090255 according to the manufacturer's protocol.

#### Rat Neurons

Total RNA was isolated from dissociated neurons using the RNeasy Mini Kit (QIAGEN) with in-column DNase (QIAGEN) digestion or the Illustra RNAspin Mini kit (GE Healthcare) with on-column DNase (GE Healthcare) digestion. cDNA was synthesized using MuLV reverse transcriptase (Promega), random primers (Promega), oligo dT primers (Promega), and RNase inhibitors (Thermo Scientific). qPCR was performed using iTaq Universal Sybr Green Supermix (BioRad) and the BIO-RAD CFX Connect realtime PCR Detection System or the PerfeCTa SYBR Green FastMix (Quantabio). To measure pre-mRNA, primers that target intron-exon borders served for cDNA synthesis and subsequent amplification (14 cycles) using the manufacturer's protocol in the One-Step RT-PCR kit (QIAGEN). The amplified product level was quantified by qPCR using the same primers. Pre-mRNA primers are in [Table S6](#) (Saha et al., 2011).

### NanoString

NanoString probes were designed for indicated pre-mRNAs ([Table S4](#)) by NanoString technologies, and assays were performed following the manufacturer's protocol.

### RNA Sequencing

#### General Protocol

Before library preparation, for capture experiments, ERCC spike-in RNA (Ambion) was added to RNA samples according to the instruction of the manufacturer. Libraries were prepared using the High Throughput Total RNA TruSeq kit (Illumina), following the instructions of the manufacturer but scaling down all volumes to 1/3 of the recommended volumes. Libraries were sequenced on a NextSeq 500 (Illumina) to a depth of at least 30 million reads per library for total RNA-seq, 20 million reads per library for eRNA-seq and 3 million reads per library for ARG-seq. We aligned reads to the mm9 genome using the STAR aligner (Dobin et al., 2013) and then made the resulting SAM files into BED files using SAMtools and BEDtools (Li et al., 2009; Quinlan and Hall, 2010). We used UCSC-tools (Kuhn et al., 2013) to make bigWig files for viewing on the genome browser. We used bedtools map to count reads in both exons and introns. We then analyzed the raw count data using R, including edgeR (Robinson et al., 2010).

#### ARG-Seq Probe Design Synthesis

For ARG-seq, capture probes were designed as oligonucleotides tiling activity-regulated exons and control exons. Genes to be captured were 251 ARGs that showed a reproducible 3.5-fold increase in transcription at either 1 or 6 hr of KCl treatment in two replicates of published RNA-seq data (Kim et al., 2010) and 47 genes that showed no change with KCl but spanned a range of expression values (controls). Synthesized probes were 100 base pairs in length, with each probe overlapping the previous probe by 76 base pairs ([Table S1](#)). Probes had PCR primer binding sites and IVT promoters added. These oligonucleotides were ordered from Custom Array, PCR-amplified, and transcribed *in vitro* into biotinylated RNA baits using the Megascript SP6 *In Vitro* Transcription kit (ThermoFisher).

#### eRNA-Seq Probe Design and Synthesis

For eRNA-seq, capture probes were designed as oligonucleotides tiling putative activity-regulated enhancers, which were identified based on their location relative to ARGs and their transcription factor binding. To identify these putative enhancers, we started with all CREB, SRF, CBP, NPAS4, or Pol2 binding sites from a previous study (Kim et al., 2010). We then took only those sites that were within 100kb of a transcription start site of one of the ARGs used in our ARG-seq experiments. We chose this threshold because 80% of enhancers regulate transcription start sites (TSSs) within 100kb (Chepelev et al., 2012). We eliminated intragenic enhancers and those located within 1kb from the transcription end site or 500bp from the transcription start site of a gene. We designed probes to span the entire TF-bound putative enhancer, plus 500bp on each side. Synthesized probes were 99 base pairs in length, with each probe overlapping the previous probe by 73 base pairs ([Table S1](#)). This oligonucleotide library was ordered from Twist Biosciences. We amplified and *in vitro* transcribed the RNA baits as described above for the ARG-seq baits. We also designed probes to tile the ERCC spike ins (Ambion) that were designed and ordered with our eRNA capture oligonucleotides. ERCC spike in oligonucleotides were made with different PCR adaptors so that they could be amplified and *in vitro* transcribed separately.

#### Capture

For ARG-seq and eRNA-seq, samples were treated in the same manner as with total RNA-seq, except that after library preparation, 250ng of pooled libraries were heated to 95°C to denature DNA and then incubated with 250ng ARG-seq or eRNA-seq RNA baits (plus ERCC baits in a volume to allow for equal molar ratios of all probes) overnight at 65°C in hybridization buffer (2.5ug Cot1 DNA (ThermoFisher), 2.5ug Salmon Sperm DNA (ThermoFisher), 15mM p5 blocking primers, 15mM p7 blocking primers, 5X SSPE (ThermoFisher), 5X Denhardt's Solution (ThermoFisher), 0.133% SDS). Blocking primers are: p5-AATGATACGGCGACCACC

GAGATCTACAC, ACACTCTTCCCTACACGACGCTTCCGATC/3InvdT/ p7-CAAGCAGAAGACGGCATACGAGAT, GTGACTGGA GTTCAGACGTGT GCTCTCCGATC/3InvdT/ Primers for amplification are: p5-AATGATAACGGCGACCACCGAGA, p7-CAAGCAG AAGACGGCATACGAG.

Hybridized samples were incubated with MyOne Streptavidin T1 Dynabeads (Invitrogen) in binding buffer (1M NaCl, 10mM Tris-HCl pH 7.5, 1mM EDTA). Beads were washed once in 1x saline-sodium citrate (SCC), 0.1% SDS at room temperature and three times in 0.1x SCC 0.1% SDS at 65°C. Captured libraries were eluted with 0.1M NaOH and neutralized with 1M Tris-HCl pH 7.5. Libraries were then purified using the QIAGEN MinElute PCR cleanup kit and re-amplified using Herculase II Fusion polymerase (Agilent).

#### **Capture-Seq Processing and Normalization**

Data were normalized by the geometric mean of the reads from control genes or enhancers. Control regions were identified as regions that do not change with KCl in published RNA-seq data (Kim et al., 2010). ERCC spike-ins confirmed that capture occurred with similar efficiency across initial RNA concentrations.

#### **Fiber Photometry**

##### **Viral Injection and Optic Fiber Placement**

To monitor bulk activity of neurons in mouse primary visual cortex (V1), mice were anesthetized with isoflurane in 100% O<sub>2</sub> (induction, 3%–5%; maintenance, 1%–2%), and placed on a heating pad (CWE) in a stereotaxic apparatus (KOPF). Ophthalmic ointment (Puralube) was applied to the eyes. We expressed a genetically encoded calcium indicator via viral injection (0.2 μL per hemisphere of AAV1.Syn.GCaMP6s.WPRE.SV40, Penn Vector Core) bilaterally into V1 (coordinates relative to Bregma: AP: –3.6 mm; ML: +/– 2.9 mm; DV: 250 μm and 500 μm below the pial surface, via a burrhole).

Two weeks after viral injection, mice were again anesthetized with isoflurane in 100% O<sub>2</sub> (induction, 3%–5%; maintenance, 1%–2%), and optic fibers (400 μm diameter, NA 0.48) were implanted bilaterally at the injection sites (150 μm below pial surface). Mice were allowed to recover for at least 10 days prior to recording.

##### **Fiber Photometry Recordings of Bulk Calcium Activity from V1**

For photometry recordings, we delivered blue light via an LED (Plexon LED Driver PLexBright LD-1, 20 μW output, calibrated prior to each recording session) and patch cable (Doric). Recordings demonstrated very similar visual responses from each hemisphere, so data from a single hemisphere was used per mouse.

##### **Experimental Paradigm during GCaMP6 Recordings**

We used the following visual stimulation paradigm during recordings. Singly housed mice at the end of their 12-hr dark cycle (~7 am) were fitted with a patch cable for photometry recordings and moved, together with their home cage, to a light- and sound-isolated cabinet. The cabinet was initially fully dark, other than IR illumination (light source: HTX-F5-48-23), used for concurrent collection of videography to track mouse locomotion using a IR-sensitive camera (Flea3 1.3 MP Mono USB3 Vision camera, FL3-U3-13Y3M-C; Lens: H2Z0414C-MP).

Recordings were collected in darkness for 1 hr prior to bright light illumination of the homecage (two GE White 18" Fluorescent Light Fixtures, part # UCF18P and F15T8, 15W/60Hz) placed on either side of the mouse home cage. For the subsequent 3 hr, the cage was illuminated with the visual stimulation paradigm described above. Black heat-shrink tubing was used to prevent room light from affecting photometry signals. We confirmed that contamination of photometry signals by illumination of the cage was negligible, by recording photometry signals in the absence of delivery of blue light via the patch cable at the end of each recording session.

All photometry signals and timestamps from stimulus delivery and videography were acquired on a standard PC and data acquisition board (National Instruments).

#### **Histology**

In a subset of experiments (4/8), fiber localization was confirmed histologically to be in area V1 and among strongly GCaMP6-expressing cell bodies. Mice were given an overdose of tribromoethanol, perfused with 10% formalin, and brains were cut in 40 μm coronal sections and stained with 4'-6-diamidino-2-phenylindole (DAPI) to visualize nuclei. Sections were then imaged on a digital slide scanner (Olympus VS120).

#### **Western Blotting**

##### **Mouse Cortical Neurons**

To detect protein expression in mouse cortical neurons, neurons were collected in cold lysis buffer (for pERK and ARC western blots – 1% Triton X-100, 50 mM HEPES, pH 7.4, 150 mM NaCl, 1.5 mM MgCl<sub>2</sub>, 1 mM EGTA, 10% glycerol, and freshly added protease and phosphatase inhibitors from Roche Applied Science Cat. # 05056489001 and 04906837001; for pElk-1 western blots – RIPA buffer (10mM Tris pH 7.4, 1% NP-40, 150mM NaCl, 0.1%SDS, 1mM EDTA, 1mM Na(3)VO(4), 0.1% Sodium Deoxycholate) with protease and phosphatase inhibitors). Lysed neurons were mixed 3:1 with 4X sample buffer (40% glycerol, 8% SDS, 0.25M Tris-HCl, pH 6.8, 10% 2-mercaptoethanol) and boiled for 5 min. Samples were centrifuged at full speed for 3 min before loading on NuPage 4%–12% Bis-Tris Gels (Invitrogen). Gels were run at 140V for 55 min. We transferred onto nitrocellulose membranes using the BioRad transfer system at 114V for 1 hr and 7 min. Membranes were blocked in 5% milk-Tris-buffered saline + Triton X-100 (TBST) for 1 hr. They were treated with primary antibody in 5% milk-TBST for at least 1 hr at room temperature or overnight at 4°C.

4°C. To visualize protein, blots were incubated with secondary antibody in TBST in the dark for 45 min. Blots were imaged using a Li-Cor Odyessy and quantified using ImageJ. Primary antibodies used were: rabbit anti-phosphoERK1/2 (Cell Signaling Technology 4370, 1:1000), mouse anti-GAPDH (Pierce, GA1R, 1:10000), rabbit anti-ARC (Synaptic Systems, 156-003, 1:1000), mouse anti-pElk-1 (Santa Cruz, sc-8406X, clone B4, 1:1000), rabbit anti-GAPDH (Cell Signaling D16H11, 1:1000). Secondary antibodies used were: IDR dye 680 goat anti-rabbit (Li-Cor, 1:10000), IDR dye 800 goat anti-mouse (Li-Cor, 1:10000).

#### Rat Cortical Neurons

To detect protein expression in rat cortical neurons, neurons were disrupted by brief sonication (three cycles of 30 s in low setting in Bioruptor at 4°C) and then cleared of debris by high-speed centrifugation (14500 RPM for 1 min). The supernatant was collected in separate tubes and resolved by gel electrophoresis on 4%–20% pre-cast gels (Life technology) and transferred to a nitrocellulose membrane using the iBlot gel transfer apparatus (Life technology). Immunoblots were incubated with primary antibody overnight. Blots were visualized with a Li-Cor Odyssey infrared scanner after immunolabeling primary antibodies with Goat anti-Mouse IgG (H+L) Cross-Adsorbed Secondary Antibody, Alexa Fluor 680 (ThermoFisher). Images were processed using the Odyssey 2.1 software. Primary antibodies used were: rabbit anti-phosphoERK1/2 (Cell Signaling Technology 4370), H4 (Cell Signaling Technology 2935), Actin (Millipore, AM4302).

#### Nuclear Isolation

Nuclear lysate was prepared from treated neurons by first liberating the nuclei in a non-ionic detergent buffer (10mM HEPES pH 7.9, 10mM KCl, 2mM MgCl<sub>2</sub>, 0.5mM dithiothreitol, 0.1% NP-40) for precisely 30 s and subsequently lysing them in NETN buffer (0.5% NP-40, 1mM EDTA, 50mM Tris, 120mM NaCl, pH 7.5) freshly supplemented with 0.5% protease inhibitor cocktail (Sigma) and phosphatase inhibitor cocktails (Sigma). Nuclear liberation was confirmed under the microscope before the released nuclei was scraped and dissolved in the NETN buffer.

#### Immunocytochemistry

To detect nuclear phospho-CaMKIV levels, after stimulation, neurons were fixed in 4% PFA for 15 min. Neurons were then washed twice in PBS and blocked and permeabilized for 30 min using 1% BSA in PBS + 0.25% Triton X-100 (BSA-PBST). Neurons were then incubated overnight at 4°C in BSA-PBST and phospho-CaMKIV antibody (1:500, Santa Cruz sc-28443-R). They were then washed 3 times with PBS and incubated for 1 hr at room temperature in secondary antibody (1:1000 ThermoFisher, R37117). They were then washed once with PBS, incubated for 10 min with DAPI (Roche, 10236276001) in PBS, and washed again with PBS. Neurons were imaged with a Leica inverted microscope. Images were taken with LAS software and quantified using ImageJ.

#### Chromatin Immunoprecipitation

Media on the neurons was removed and neurons were fixed in crosslinking buffer (10 mM HEPES pH 7.5, 100 mM NaCl, 1 mM EDTA, 1 mM EGTA, 1% formaldehyde) for 10 min at room temperature, and this reaction was quenched using 125mM glycine for 5 min. For H3K27ac ChIP, 250,000 neurons were used per ChIP sample. For Pol2 ChIP, 2 million neurons were used per sample. Neurons were then washed with cold PBS and then collected in PBS with 0.25% BSA and pelleted by centrifuging at 700 x g for 15 min. Cell pellets were stored at -80C. Neurons were sonicated using a Covaris E3 sonicator in lysis buffer (10 mM Tris pH 8.0, 1mM EDTA, 1 mM EGTA, 1X Roche complete EDTA-free protease inhibitors, 0.15% SDS). Sonication was done for 8 min per sample with 200 cycles/burst, a 2% duty cycle at power level 3. This reliably produced fragments between 100 and 700bp in length. Samples were then supplemented with ChIP Buffer so that they were in SDS-ChIP buffer (10 mM Tris pH 8.0, 0.1% SDS, 1% Triton X-100, 150 mM NaCl, 1 mM EDTA, 0.3 mM EGTA, 1X Roche complete EDTA-free protease inhibitors). For H3K27ac ChIP, Protein A beads (Dynabeads) were washed with 1% BSA/TBST and added to the fragmented DNA for a pre-clear and rotated at 4°C for 1 hr. A different set of protein A beads was pre-treated with 0.48ug of antibody (Abcam, ab4729)/sample for H3K27ac ChIP. The same procedure was followed for Pol2 ChIP, but with Protein G Dynabeads and 4ug antibody (Abcam, ab817) per crosslinked input. Following the pre-clear, pre-clear beads were removed, an aliquot of fragmented DNA was set aside as the input, and antibody-treated beads were incubated with the fragmented DNA overnight at 4°C. After overnight incubation, beads were washed twice with cold low salt wash buffer (0.1% SDS, 20 mM Tris pH 8.0, 1% Triton X-100, 150 mM NaCl, 2 mM EDTA), twice with cold high salt wash buffer (0.1% SDS, 20 mM Tris pH 8.0, 1% Triton X-100, 500 mM NaCl, 2 mM EDTA), twice with cold LiCl wash buffer (1% NaDOC, 10 mM Tris pH 8.0, 1% NP40, 250 mM LiCl, 1 mM EDTA), and once with room temperature TE. Crosslinks were reversed by incubating samples in TE+1%SDS at 65°C overnight. Samples were then treated with RNase A (Ambion) and Proteinase K (New England Biolabs), and DNA was eluted using MinElute Columns (QIAGEN) according to the instructions of the manufacturer.

#### Chromatin Immunoprecipitation Sequencing

##### H3K27ac ChIP-Seq

For H3K27ac ChIP-seq, libraries were prepared using 5μg of immunoprecipitated DNA or input DNA with the NuGen Ultralow V2 1-96 library prep kit. Libraries were sequenced on an Illumina NextSeq500 to a depth of at least 30 million reads per library. Reads were aligned to mouse genome mm9 using bowtie2 ([Langmead and Salzberg, 2012](#)). The resulting SAM files were made into BED files using SAMtools and BEDtools, with reads extended to 300 base pairs ([Li et al., 2009; Quinlan and Hall, 2010](#)) and then into bigWig files using UCSC-tools ([Kuhn et al., 2013](#)). Reads were assigned to individual enhancers or promoters using bedtools map and data were analyzed using R.

For downstream analysis, H3K27ac ChIP-seq data were input-normalized and then normalized by dividing by the geometric mean of control enhancers identified based on their location near the same control genes used for ARG-seq (control enhancer selection described in Capture RNA sequencing section). The data used for plotting (Table S7) included the mean input-normalized and control-normalized signal from the same regions targeted by eRNA-seq of each enhancer for two biological replicates, averaging each enhancer across replicates prior to plotting, and including only enhancers captured in eRNA-seq. Plots in Figures S4 and S8 were made as described in the “Published ChIP-seq data” section (see below).

### **Pol2 ChIP-Seq**

For Pol2 ChIP-seq, reads were aligned to mouse genome mm9 using the STAR aligner (Dobin et al., 2013). The resulting SAM files were made into read-extended (200 bases per fragment) BED files using SAMtools and BEDtools (Li et al., 2009; Quinlan and Hall, 2010) and then into bigWig files using UCSC-tools (Kuhn et al., 2013). For analysis, the metaseq (Dale et al., 2014), numpy (Van Der Walt et al., 2011), and matplotlib (Hunter, 2007) python packages were used to process aligned bam files and to produce read-depth- and input- normalized data. TSS positions were obtained from UCSC gene annotations and Refseq gene databases (see Table S8). For two genes (*Amigo3*, *Dusp5*), we used Refseq TSSs that are now deprecated. The mean Pol2 density at each TSS was measured using 600bp windows centered (-300bp to +300bp) on the TSS. ARG gene lists were filtered for a single TSS per gene, using the TSS with greatest average Pol2 density of all samples within single biological replicate. Additional analysis was performed in R. Given across-sample variability in read-depth- and input-normalized data, the samples were further normalized to Pol2 ChIP-seq density measured at constitutively active, non-activity-regulated control gene promoters—similar to the across-sample ChIP-seq normalization methods adopted by others for quantitative analysis of peaks (Shao et al., 2012). Specifically, data from each sample was normalized to the median value of a distribution of Pol2 density values occurring at ~800 constitutively active TSSs (-300 to +300bp) with unchanging mRNA levels under KCl as measured by RNA-seq (Kim et al., 2010).

### **Published ChIP-Seq Data**

For analysis of published data, data from Kim et al. (2010) was used as aligned and processed by the authors and downloaded from GEO as bigWig files. Data from Telese et al. (2015) was downloaded from GEO as fastq files, re-aligned to mm9 using bowtie2, and processed like the H3K27ac data in this study. Data from ENCODE was downloaded as bigWig files as processed by the authors. Signal was binned across TSSs and enhancers and input-normalized using the Python package metaseq (Dale et al., 2014). Plots were made using R, smoothing with the lowess function.

### **Luciferase Assays**

The sequences for enhancer e5 was amplified using PCR from genomic DNA extracted from wild-type (C57BL/6J) mice, utilizing primers that included flanking KpnI and Xhol sites (ATACGGTACCCGAGACTACGTCA, ATGTCTCGAGATTAAAAAGGCC). These amplified sequences were cloned into pTAN02, an ITR-containing AAV screening vector containing minimal human pFos upstream of the Firefly luciferase gene (Nguyen et al., 2016) with the KpnI and Xhol sites. Additionally, pTAN02 without an enhancer insert was included as a “no enhancer” control. Primary cortical neuron cultures (see above) were transfected using PEI (4:1 PEI:DNA mass ratio) on DIV5. These cultures were co-transfected with an internal control Renilla luciferase construct, pTK-RN, at a fixed mass ratio of 9:1, Firefly construct:Renilla construct. Each experiment was run in triplicate. Cultures were depolarized on the morning of DIV7 as above for 12 hr. A non-depolarized control received a media change with no additional KCl. Cultures were collected on the night of DIV7 and prepared using the Dual-Luciferase Reporter Assay System (Promega) according to the manufacturer’s protocol. The lysate was assayed over a 10-s period using the GloMax 20/20 Single Tube Luminometer (Promega), and the luciferase activity was calculated as a ratio of the Firefly to Renilla output values.

### **QUANTIFICATION AND STATISTICAL ANALYSIS**

We have included most statistical details in our Figure legends, including p values, statistical tests used, ‘n’s for each experiment, and a description of to what ‘n’ refers. Biological replicates refer to biological material from different mice (all experiments), with biological replicate samples also collected on a different day (*in vitro* experiments only).

### **Gene Classification**

#### ***In Vitro***

In experiments in mouse cortical neurons, our gene lists consisted of genes that showed significant induction (FDR < 0.05) of at least 1.5-fold at any time point in ARG-seq experiments, as determined by edgeR (173/251 captured ARGs). We classified genes as PRGs if they showed less than a 2-fold reduction in expression in 6 hr-KCl-treated neurons in the presence of cycloheximide. SRGs showed a greater than 2-fold reduction in the presence of cycloheximide (FDR < 0.05 by edgeR). We classified PRGs as rapid if they had higher induction at 1 hr compared to 6 hr and delayed if they had higher induction at 6 hr compared to 1 hr. All rapid PRGs showed >2-fold pre-mRNA induction by 20 min of stimulation. We eliminated four PRGs from our analysis due to ambiguity in our classification scheme, which exclusively relied upon kinetics of induction to distinguish rapid from delayed PRGs. We eliminated two genes (*Vgf* and *Homer1*) because their expression peaked at 6 hr of KCl stimulus, but they showed robust and significant pre-mRNA induction at 20 min. We also eliminated two genes (*Gadd45b* and *Nfkbid*) because while their mRNA induction peaked at 1 hr, they did not show a trend toward pre-mRNA or mRNA induction at 20 min of KCl. For significance testing in the classification, we used edgeR’s glmFit

and glmTreat functions (Robinson et al., 2010). Principal-component analysis (PCA) was performed using the prcomp function in R using normalized mRNA expression values. Specifically, to better assess expression kinetics, each gene was normalized such that its lowest expression value was set at 1 and its highest at 10.

### In Vivo

For *in vivo* data in Figure 4, gene classification was based on *in vitro* mouse data. However, we eliminated dPRGs with higher induction at 30 min compared to 150 min of visual stimulus.

### Functional Annotation

Functional annotation was performed using PANTHER version 13.1 (Mi et al., 2017) (Table S5). Text of the table reflects output from the program with duplicate entries deleted. Colors in table represent manual classification. Genes were identified as directly regulating transcription if they were annotated as transcription factors/cofactors or as binding to DNA. Genes were identified as indirectly regulating transcription if they were annotated as part of a signaling pathway likely to regulate transcription. Genes were also identified as indirectly regulating transcription if they are not channels, receptors, or secreted proteins that were annotated as regulating transcription but not as transcription factors or binding to DNA.

### Nearest-Neighbor Classifier

Our first classifier for post hoc determination of *in vitro* activity pattern based on *in vitro* gene expression used the maximum expression at any time point for each gene, such that the kinetics of gene induction did not contribute to the classifier. It compared each replicate in a testing set to all replicates in a training set using Euclidean distance and classified based on the minimum distance. It was run with both separate testing and training sets (6 biological replicates each, randomly sorted) and leave-one-out cross validation. This classifier was run using all genes targeted by ARG-seq, only induced ARGs, and only control (non-ARG) genes.

Our second classifier tested *in vivo* activity pattern and was trained using *in vitro* gene expression. We used 60-min time points for both training and testing sets to enable detection of both rPRGs and dPRGs. The 11 ARGs used were *Egr1*, *Fos*, *Bdnf*, *Npas4*, *Cdkn1a*, *Crem*, *Grasp*, *Maml3*, *Scg2*, *Pcsk1*, and *Egr2*. To compare expression without influence of the absolute magnitude of expression, which differs between *in vivo* and *in vitro* experiments, data for each experiment (i.e., *in vitro* or *in vivo*), was quantile normalized between genes. The classifier then compared each replicate in the *in vivo* testing set to all replicates in the *in vitro* training set using Euclidean distance and classified based on the minimum distance.

### scRNA-Seq Analysis

#### Data

We used raw scRNA-seq (inDrops method) expression values from neurons in the visual cortex that had been exposed to 0, 1 or 4 hr of sustained visual stimulation (Hrvatin et al., 2018). We limited our analysis to only neurons classified with high confidence as excitatory neurons by Hrvatin et al (2018). Our analysis was done on data from  $n = 4$  individual visual cortices for each time point pooled together.

#### Activity History Inference

Briefly, to infer activity history, each gene in each neuron at 1 hr was first called as ON or OFF based on the distribution of expression of that gene in excitatory neurons from the unstimulated visual cortex (Figure 2C). Next, the numbers of rPRGs and dPRGs that were ON or OFF in each cell were summed. The number of genes ON in each gene class was used to determine whether that class as a whole was ON or OFF, based on thresholds set using data from unstimulated neurons (see below). The rPRG and dPRG states were then used to infer activity history as inactive (or unchanged from unstimulated), BRIEF, or SUSTAINED in response to visual stimulation.

A detailed description: For this analysis we used read-depth normalized data. We started by determining whether each rPRG or dPRG was induced in each neuron. A gene was defined as induced in a neuron from the stimulated cortex if its expression in that neuron was greater than a threshold set based on the expression of that gene in neurons from unstimulated cortex. This threshold was set at the 95<sup>th</sup> percentile of expression values for that gene in all the excitatory neurons in unstimulated cortex.

We then used these classifications of individual genes to determine whether neurons induced our gene classes (i.e., rPRGs or dPRGs) as a whole. We counted the number of rPRGs and dPRGs induced in each neuron. We set a threshold for the number of genes in each class that needed to be induced for that class to be considered ON in the neuron. We determined this threshold separately for rPRGs and dPRGs. To determine this threshold, we compared distributions of rPRG or dPRG metagenes between the stimulated and unstimulated samples. rPRG and dPRG metagenes were summed expression of all rPRGs or dPRGs, respectively, in each cell. We specifically compared metagene distributions between stimulated OFF neurons (i.e., neurons in the stimulated cortex for which the class is OFF) and unstimulated neurons (i.e., neurons from the unstimulated cortex), as our goal was for the stimulated OFF neurons to be similar to the unstimulated neurons to ensure that the class is actually OFF in stimulated OFF neurons. The threshold was therefore set as the maximum number of genes induced in the class for which the distribution of metagene expression for the stimulated OFF neurons was the same as or slightly left-shifted (i.e., less expressed) compared to the unstimulated neurons. More specifically, the threshold was set at the number of genes induced in the class that produced the minimum distance between distributions where  $p > 0.1$  by the Kolmogorov–Smirnov test and the stimulated OFF distribution was left-shifted from the unstimulated distribution.

We defined BRIEF neurons as having rPRGs ON and dPRGs OFF, SUSTAINED neurons as having dPRGs ON, and inactive neurons as having rPRGs and dPRGs OFF. For most classification of BRIEF and SUSTAINED neurons, we used the lists of rapid PRGs and delayed PRGs defined in [Figure 1](#) of this paper. We also defined dPRGs among significantly induced genes in the *in vivo* data: dPRGs showed significant induction at 4 hr (FDR < 0.05, 2-fold induction, unpaired, two-sided rank-sum test on bulk neurons) and similar (< 1.4 fold different) expression at 1 hr and 4 hr following stimulus. In this analysis, we defined genes for each layer individually.

For the analyses to determine whether the population of BRIEF neurons was significant, we asked whether BRIEF neurons were responding to the visual stimulus or reflective of an expected proportion of rPRG-expressing cells among unstimulated neurons. We compared neurons from the stimulated cortex classified as having dPRGs OFF to unstimulated neurons. We used a Fisher's exact test to assess enrichment for rPRG-ON cells among dPRG-OFF cells compared to unstimulated cells, expecting an odds ratio not equal to 1 if there was a difference in the proportion of BRIEF neurons between dPRG-OFF neurons and unstimulated neurons. We performed this analysis on all excitatory neurons together as well as for each layer individually.

#### **Differential Gene Expression Analysis**

Differential gene expression analysis was performed using an unpaired, two-sided Wilcoxon rank-sum test comparing all BRIEF neurons to all SUSTAINED neurons. We confirmed that the package Monocle2 ([Trapnell et al., 2014](#)) gave us identical results. We also performed DE analysis using DECENT ([Ye et al., 2017](#)) and used it to generate imputed read counts. DECENT had greater power to detect differentially expressed genes, but revealed similar trends (i.e., differential expression of deep layer markers in BRIEF neurons).

#### **RNA-Seq**

##### **Expression Analysis**

We quantified pre-mRNA transcription using intron reads from total RNA-seq data ([Gaidatzis et al., 2015](#); [Gray et al., 2014](#)).

For ARG-seq and total RNA-seq figures, we plotted a mean of the control-normalized expression levels for each gene from several biological replicates. All p values reported in the figure legends for comparisons between two groups of genes are from an unpaired non-parametric two-tailed Wilcoxon rank-sum test (unless otherwise noted). A paired test was used when comparing between the same set of genes in two conditions. We confirmed significance using a two-tailed Student's t test (log-normalized if comparing fold-inductions). We also confirmed that the differences observed via analysis of the mean expression levels were replicated in each biological replicate individually ( $p < 0.05$ , rank-sum test).

For ARG-seq and eRNA-seq, we confirmed using the Tukey HSD test in conjunction with ANOVA that expression from control genes or control enhancers in read-depth-normalized samples and spike-in-normalized samples is not affected by membrane depolarization, visual stimulation, or addition of U0126/SL327 (adjusted  $p > 0.8$ ).

##### **Comparison to Other Gene Lists**

Comparison between the genes induced in our study *in vitro* and the genes induced in three *in vivo* brain studies was performed with lists generated in a previous study ([Cho et al., 2016](#)). Comparison between the genes induced in our study *in vitro* and the genes induced in mouse macrophages and human cancer cell lines was performed using gene lists of induced genes generated by the authors of the previous studies ([Escoubet-Lozach et al., 2011](#); [Tullai et al., 2007](#)). Human cancer cell line genes were converted to their mouse orthologs using the Mouse Genome Database ([Blake et al., 2017](#)) prior to analysis.

#### **Analysis of Photometry Signals**

All data analysis of GCaMP6 photometry signals was performed in MATLAB (Mathworks). For estimating the time course of changes in V1 calcium activity during each presentation of a 60 s lights-on stimulus onset (and during the first hour of recording in the dark, during 'pseudo-trials' in which the light was not actually switched on), we first estimated the mean GCaMP6 fluorescence in the 10 s period prior to stimulus onset,  $F_0$ . We then calculated the fractional change in fluorescence at each time point from -20 s to 80 s relative to stimulus onset, as  $(F(t) - F_0)/F_0$ .

#### **ChIP-Seq**

##### **H3K27ac**

We confirmed using the Tukey HSD test in conjunction with ANOVA that read-depth-normalized signal at control enhancers was not affected by stimulation or by addition of U0126 (adjusted  $p > 0.8$ ). We also performed one replicate using *Drosophila* spike-in chromatin (Active Motif #61686, #53083) according to the instructions of the manufacturer and observed that U0126 treatment did not result in global H3K27ac changes. The plots shown only include enhancers that showed an increase in H3K27ac with neuronal activity: 248 of the 940 putative enhancers reproducibly gain H3K27ac within the first hour of stimulation in two biological replicates (> 1.3 fold change). All p values reported are from the two-tailed non-parametric Wilcoxon rank-sum tests, but we confirmed significance using the Student's t test. Unpaired tests were used if comparing between two groups of enhancers, and paired tests were used if comparing between the same group of enhancers in two conditions. We also performed a Student's t test comparing the mean signal across all enhancers from each replicate for each gene class without U0126 to the mean signal across enhancers from each gene class with U0126 and found no significant difference ( $p > 0.6$ ). We also compared each enhancer individually, and again found no significant change in H3K27ac signal at any enhancer with U0126 ( $p > 0.9$ , Bonferroni corrected).

**Pol2**

Additional analysis was performed in R. As a separate analysis, rPRG and dPRG TSS lists were filtered for TSSs with mean Pol2 ChIP-seq density greater than a threshold condition defined as two standard deviations above the mean value of un-expressed (Kim et al., 2010) negative control TSS. For fold change analysis, fold change was calculated at each TSS using the average unstimulated Pol2 density value obtained from two DMSO- and two U0126- treated samples.

**Published ChIP-Seq Data**

For the enhancer data, in addition to the data shown in the figures, we also compared only those rapid and delayed enhancers near dPRGs. In unstimulated neurons, for SRF, CREB, MEF2, MED23, MED1 and NCoR, we compared binding –6kb to +6kb from the centers of rapid enhancers compared to delayed enhancers and as reported in the main text found greater binding at rapid enhancers ( $p < 0.009$ , rank-sum test, including only enhancers within 100 kb of dPRGs). Active histone marks H3K27ac, H3K4me2, H3K4me1, and H4K16ac were also higher in a comparison of the same rapid compared to delayed enhancers in unstimulated neurons ( $p < 0.01$ , rank-sum test, only enhancers within 100 kb of dPRGs).

**DATA AND SOFTWARE AVAILABILITY**

The accession number for the RNA-seq and ChIP-seq reported in this paper is GEO: GSE111899.